21 SEPTEMBER UNIVERSITY
OF MEDICAL & APPLIED SCIENCES
Deanship of Environment and Community Service
Medical Center for Training and Rehabilitation

جامعة ٢١ سبتمبر للعلوم الطبية والتطبيقية
عمادة البيئة وخدمة المجتمع
المركز الطبي للتدريب والتأهيل

Radiological Evaluation of Brain and Skull Tumors Using Computed Tomography

A Research submitted for partial fulfilment for the Requirements of Diploma degree in Diagnostic Radiologic

Prepared by researchers

Abrar Adel Mohammed Al-Sharji

Suad Mohammed Qasim Al-Qasimi

Doaa Hussein Ahmed Al-Okad

Samat Saleh Mohammed Al-Dhabri

Najla Najib Ahmed Al-Hazmi

Walaa Ahmed Mohammed Al-Ghazali

Rudaina Abdul Wahid Al-Sheikh

Younes Abdullah Mohamed Al Qadri

Supervisor

Dr.Ibrahim Al-Hamadi

Dr. Noor Aldeen Al-Fakih

2025-2026^{AD}

Dedication

To the nothing, to the lack of support and the children of the streets and the desert, to the abandoned by his relatives, to everyone who has no dear, to those who are not contained by the gifts of others, to everyone whom life has wracked and made him to the bottom of a bastard, to the miserable and toiling, To those in the darkness waiting for the break of dawn to the poor, to all those who are awakened, to the poor who are panting after a morsel of subsistence to fill the number of their children, to the women and men of the fields who revive the earth after its death, to those who are stranded in hospitals looking on, to their dying relatives Powerless, to those who do not have the price of medicine and food, to my soul that has endured so much.

Acknowledgements

This research project would not have been done without ALLAH and the support of many people.

Our deepest gratitude to our supervisor **Dr. Noor Aldeen Al_Fakih** for his encouragement, Support and guidance and **to Dr. Ibrahim Al-Hamadi** for his great support and Evaluation in this research.

Our warmth gratitude and thanks to Diagnostic Radiology Department staff in 21 September University for Medical & Applied Faculty of Applied Medical Sciences & Radiology Department & MCTR and to National Oncology Center - SANA'A - CT Scan Departmental who facilitated to getting the sample of this work.

Table of Contents

List of Tables

List of figure

List of abbreviations

Term	The meaning
ALARA	As Low As Reasonably Achievable
ANOVA	Analysis of Variance
ASCO	American Society of Clinical Oncology
BBB	Blood–Brain Barrier
CA	Carcinoma
CISS	Constructive Interference in Steady State
CM	Contrast Medium
CN	Cranial Nerve
CNS	Central Nervous System
CPA	Cerebellopontine Angle
CSF	Cerebrospinal Fluid
CT	Computed Tomography
DSA	Digital Subtraction Angiography
DWI	Diffusion-Weighted Imaging
F	Female
F:M	Female to Male ratio
FDG-PET	Fluorodeoxyglucose-Positron Emission Tomography
IAC	Internal Auditory Canal
ICA	Internal Carotid Artery
IDH	Isocitrate Dehydrogenase
IRB	Institutional Review Board
JDPO	Journal of Diagnostic Performance in Oncology
kVp	Kilovoltage Peak
M	Male
MDCT	Multi-Detector Computed Tomography
MPR	Multiplanar Reconstruction
MRA	Magnetic Resonance Angiography

MRI	Magnetic Resonance Imaging
N	Total number of subjects in a sample or subgroup
n	Number of subjects within a specified subgroup
NF2	Neurofibromatosis Type 2
NOC	National Oncology Center
NPV	Negative Predictive Value
p	p-value (probability value)
PFT	Posterior Fossa Tumor
Ppm	Parts Per Million
PPV	Positive Predictive Value
r	Correlation coefficient
RCC	Renal Cell Carcinoma
SCC	Squamous Cell Carcinoma
SD	Standard Deviation
SPSS	Statistical Package for the Social Sciences
STIR	Short Tau Inversion Recovery
TE	Echo Time
WHO	World Health Organization
χ^2	Chi-square (statistical test)

Abstract

Background: Brain and skull tumors are major causes of neurological morbidity. In resource-limited settings like Yemen, where MRI is often unavailable, CT remains the primary diagnostic tool. However, systematic data on CT characteristics of these tumors in the Yemeni population are lacking. This study evaluates the demographic and multi-parametric CT features of brain and skull tumors at the National Oncology Center, Sana'a, Yemen.

Methods: A descriptive cross-sectional study was conducted from October 2025 to February 2026, including 52 consecutive patients (age 2–75 years) with confirmed brain or skull tumors who underwent contrast-enhanced CT. Demographic data, tumor characteristics, and CT features (density, enhancement, necrosis, calcification, edema, mass effect) were analyzed using SPSS version 23.0, with significance set at $p < 0.05$.

Results: Females predominated (65.4%). Metastatic tumors were most frequent (46.2%), followed by primary CNS tumors (40.4%); breast cancer was the leading primary source (17.3%). The cerebral region was the most common location (48.1%). Multiple lesions were significantly more frequent in metastases (54.2%) than primary tumors (28.6%) ($p=0.002$). Significant correlations included paraganglioma with iso-density ($r=0.68$) and calcification ($r=0.82$); orbital tumors with iso-density ($r=0.72$); and metastases with necrosis ($r=0.45$). Key co-occurrence patterns were strong enhancement with necrosis in metastases ($p=0.001$) and hyperdensity with calcification in meningiomas ($p=0.004$).

Conclusion: CT effectively characterizes brain and skull tumors in resource-limited settings. Distinct CT feature patterns and their statistical associations provide a basis for a preliminary diagnostic algorithm, enhancing early diagnosis and clinical decision-making where advanced imaging or histopathology is unavailable.

Keywords: Brain tumors, Skull neoplasms, CT imaging, Yemen, Resource-limited settings, Neuro-oncology, Metastatic tumors, Meningioma, Paraganglioma.

Chapter one

Introduction

1.Introduction

1.1 Background

Brain and skull neoplasms represent a heterogeneous and biologically diverse group of pathological entities that significantly contribute to neurological morbidity and mortality worldwide. These tumors encompass primary central nervous system (CNS) neoplasms, metastatic lesions, and calvarial tumors, each characterized by distinct histopathological, molecular, and radiological profiles. Accurate and timely diagnosis is critical for therapeutic decision-making, surgical planning, prognostic stratification, and overall patient survival outcomes.

Neuroimaging constitutes the cornerstone of diagnostic evaluation in neuro-oncology. Among available imaging modalities, Computed Tomography (CT) continues to play a pivotal role, particularly in emergency settings and in healthcare systems with limited access to advanced imaging technologies such as Magnetic Resonance Imaging (MRI). CT imaging offers several advantages, including rapid acquisition time, wide availability, cost-effectiveness, and superior detection of calcification, acute hemorrhage, and osseous involvement. These features establish CT as an indispensable first-line imaging modality in cranial oncology (**Atlas, 1990; Brant-Zawadzki *et al*., 1984).**

Technological advancements in CT imaging—particularly the transition from single-slice scanners to multi-detector CT (MDCT)—have markedly enhanced image quality and diagnostic capability. The 64-slice CT scanner utilized in the present study allows high spatial resolution imaging, rapid volumetric acquisition, and multiplanar reconstruction (MPR), enabling detailed evaluation of intracranial parenchyma and skull structures.

Furthermore, the intravenous administration of iodinated contrast agents improves lesion characterization by highlighting vascularity, demonstrating blood–brain barrier (BBB) disruption, and revealing enhancement patterns that aid in tumor differentiation and grading (**Smirniotopoulos *et al*., 2007; Bae, 2010).**

In recent years, neuro-oncological imaging has increasingly integrated principles from the radiogenomic paradigm, which proposes a meaningful association between imaging phenotypes and underlying genomic expression patterns **(Gillies *et al*., 2016)**. CT-derived imaging biomarkers—such as attenuation characteristics (hypodense, isodense, hyperdense, or mixed), contrast enhancement patterns, necrosis, calcification, perilesional edema, and mass effect—reflect tumor vascularity, cellular density, angiogenesis, and biological aggressiveness (**Ellika *et al*., 2007**). Systematic evaluation of these imaging characteristics may contribute to non-invasive tumor stratification and reduce reliance on invasive diagnostic procedures in selected clinical scenarios.

Globally, the epidemiological distribution of brain tumors varies according to geographic and demographic factors. Gliomas and meningiomas constitute the most common primary brain tumors in Western populations, while metastatic brain disease prevalence correlates with regional cancer incidence patterns **(Ostrom *et al*., 2020).** However, in Yemen, there remains a marked deficiency of comprehensive epidemiological and radiological data addressing brain and skull tumors. The absence of structured local imaging analyses limits evidence-based clinical decision-making.

Accordingly, this study aims to provide a systematic radiological evaluation of brain and skull tumors using CT imaging at the National Oncology Center in Sana’a, Yemen, thereby contributing foundational data to an

underrepresented population and enhancing the diagnostic utility of CT in resource-limited environments.

1.2 Problem Statement

In resource-limited healthcare systems such as Yemen, access to advanced neuroimaging modalities—particularly MRI—is often restricted due to economic, infrastructural, and logistical constraints. Additionally, histopathological and neurosurgical services may not always be readily available. Consequently, CT imaging frequently serves as the primary—and sometimes sole—diagnostic modality for intracranial and skull pathologies.

Despite this reliance on CT, there is a substantial lack of systematic, evidence-based research describing CT imaging characteristics of brain and skull tumors within the Yemeni population. The absence of locally derived radiological data leads to diagnostic uncertainty, delays in referral and treatment planning, and the inability to establish context-specific diagnostic algorithms.

This study seeks to address this gap by conducting a structured analysis of CT imaging features among patients diagnosed with brain and skull tumors at a national referral center.

1.3 Research Questions

1. What are the demographic characteristics (age and gender distribution) of patients diagnosed with brain and skull tumors in Yemen?
2. What are the most common CT imaging features observed in different tumor categories?
3. Is there a statistically significant association between specific CT imaging features and tumor types?

4. Can CT imaging features be utilized to develop a diagnostic algorithm suitable for resource-limited settings?
5. What characteristic CT patterns define each tumor category?

1.4 Justification of the Study

This study is justified for several scientific and clinical reasons:

1) There is a significant absence of structured neuroimaging data specific to the Yemeni population.
2) CT imaging remains the primary diagnostic modality in many regional healthcare facilities.
3) Developing evidence-based CT interpretation patterns can improve diagnostic accuracy and reduce delays in management.
4) Establishing locally relevant imaging characteristics enhances clinical decision-making in resource-constrained environments.
5) The study provides an educational framework for clinicians, radiologists, and trainees to refine CT interpretation skills in neuro-oncology.

1.5 Importance of the Study

The importance of this study lies in its anticipated contribution to clinical practice and scientific knowledge:

1) It enhances early diagnostic accuracy of brain and skull tumors using accessible imaging technology.
2) It supports the development of a CT-based diagnostic framework tailored to low-resource settings.
3) It provides baseline epidemiological and radiological data for future comparative studies.

4) It contributes to global neuro-oncological literature by representing an understudied population.
5) It may improve patient outcomes through optimized imaging-based triage and management planning.

1.6 Objectives of the Research

1.6.1 General Objective

To evaluate the demographic distribution and multi-parametric CT imaging characteristics of brain and skull tumors at the National Oncology Center in Sana'a, Yemen, and to determine their association with tumor categories.

1.6.2 Specific Objectives

- To document patient demographic characteristics (age and gender distribution).
- To analyze CT imaging features including density, enhancement patterns, necrosis, calcification, perilesional edema, and mass effect.
- To identify statistically significant correlations between CT imaging features and tumor categories.
- To assess diagnostic performance parameters (sensitivity, specificity, PPV, and NPV) using histopathological findings as the reference standard where available.
- To develop a preliminary CT-based diagnostic algorithm applicable to resource-limited settings.

1.7 Research Hypotheses

- H1: There are statistically significant differences in age distribution among tumor categories.
- H2: Specific CT imaging features are significantly associated with specific tumor types.
- H3: Metastatic tumors demonstrate higher rates of multiplicity and necrosis compared to primary CNS tumors.
- H4: Meningiomas are significantly associated with hyperdensity and calcification on CT imaging.
- H5: CT imaging achieves high diagnostic accuracy (>85%) in differentiating tumor types.

1.8 Definition of Terms

Computed Tomography (CT): A cross-sectional imaging modality that uses X-rays and computer processing to generate detailed anatomical images.

Enhancement Pattern: The degree and pattern of contrast uptake by a lesion following intravenous contrast administration.

Mass Effect: Displacement of adjacent brain structures due to space-occupying lesions.

Perilesional Edema: Vasogenic edema surrounding a tumor, typically appearing hypodense on CT.

Primary Brain Tumor: A tumor originating from brain parenchyma or associated structures.

Metastatic Brain Tumor: A secondary tumor arising from systemic malignancy and spreading to the brain.

1.9 Limitations of the Study

- Dependence primarily on CT imaging without routine MRI correlation.
- Limited availability of histopathological confirmation in all cases.
- Single-center study design, potentially limiting generalizability.
- Retrospective data constraints affecting completeness of clinical records.
- Potential selection bias inherent in referral-center populations.

Chapter Two

Literature Review

Chapter 2: Literature Review

2.1 Introduction

The radiological evaluation of brain and skull tumors is a cornerstone of modern neuro-oncology, providing the essential anatomical and pathological insights required to guide clinical decision-making. Computed Tomography (CT) remains a fundamental diagnostic tool, offering distinct advantages including rapid image acquisition, high availability, and superior visualization of bony structures and calcifications. This chapter provides a comprehensive review of the existing literature on the demographic patterns, topographic distribution, and multi-parametric imaging features of various brain and skull neoplasms as seen on CT. Furthermore, it explores the diagnostic performance of CT and its correlation with histopathological findings, particularly in the context of the updated World Health Organization (WHO) classification of Central Nervous System (CNS) tumors (**McNamara *et al*., 2022).**

2.2 Definition and Classification of Brain Tumors

A brain tumor is defined as a mass or growth of abnormal cells within the brain tissue. These tumors can be classified into several types that affect the brain and its associated structures. Some brain tumors are non-cancerous, referred to as benign tumors, while others are cancerous, known as malignant tumors. Brain tumors can originate in the brain itself, termed primary brain tumors, or they can begin as cancer in other parts of the body and subsequently spread to the brain, referred to as secondary, metastatic, or degenerative brain tumors **(Ohgaki & Wiestler, 2007).**

In a broader biological sense, tumors are groups of abnormal tissue cells that form lumps or mass growths. They can originate in any one of the trillions of cells in the human body and grow and behave differently depending on whether they are cancerous (malignant), non-cancerous (benign), or precancerous **(Chang *et al*., 2007).**

2.3 Tumor Behavior and Clinical Impact

The growth rate of brain tumors varies greatly and is a critical factor in determining their impact on neurological function. Both the growth rate and the precise location of the tumor determine how it affects the nervous system and can lead to dysfunction of the affected parts. The physical presence of a tumor in the brain can cause problems with various cognitive functions, including thinking, understanding, learning, attention, concentration, problem-solving, planning, and decision-making **(Chang *et al*., 2007).**

2.4 Epidemiology and Topographic Distribution

2.4.1 General and Pediatric Epidemiology

Demographic characteristics, such as age and gender, are essential factors in the differential diagnosis of intracranial lesions. The third National Cancer Survey of the United States, conducted in 1975, placed the incidence of CNS neoplasms for children younger than 15 years of age at approximately 2.4 per 100,000. This figure increased to 3.45 per 100,000 by 1994 **(Fujimoto *et al*., 2000).** Currently, the incidence of brain tumors in children is approximately 2 to 5 per 100,000 per year. Most pediatric brain tumors are primary neoplasms, as CNS metastases are rare in this population **(Nelson *et al*., 1991; Clark *et al*., 1985).** Primary CNS tumors are the most common solid neoplasms in children and represent a leading cause of cancer-related death in this demographic **(Paldino *et al*., 2011).**

2.4.2 Age and Gender Distribution

Research has consistently shown that the incidence of specific tumor types varies significantly across the lifespan. Primary CNS tumors, including certain gliomas and embryonal tumors, are more prevalent in pediatric and young adult populations, whereas metastatic disease and meningiomas are predominantly observed in older adults **(McNamara *et al*., 2022).** For instance, the mean age for metastatic tumors is often reported in the fifth and sixth decades of life, reflecting the peak incidence of primary systemic cancers such as lung and breast carcinoma (**Fink & Fink, 2013).**

Gender distribution also exhibits distinct patterns. Meningiomas demonstrate a marked female predilection, often attributed to the presence of progesterone and estrogen receptors **(New *et al*., 1980).** Conversely, certain vascular tumors like paragangliomas may show varying gender ratios depending on their genetic associations and anatomical locations **(Van Den Berg, 2005).**

2.4.3 Topographic Distribution

Topographically, the location of a lesion—whether intra-axial or extra-axial, supratentorial or infratentorial—provides significant clues to its etiology. Metastatic tumors are frequently found at the gray-white matter junction due to hematogenous spread, while primary tumors like gliomas often involve deep white matter structures **(Fink & Fink, 2013).**

2.5 Diagnosis and Medical Imaging

Most brain tumors are not diagnosed until after signs and symptoms appear. Initial diagnosis is often made by a neurologist, a specialist in disorders of the brain and central nervous system **(Clarke, 2005)**. Brain tumors can develop over varying timeframes, making them difficult to screen without radiographic imaging. Diagnosis may often be delayed, as the initial symptoms and signs tend to be vague and nonspecific. Common presenting symptoms include headache, focal seizures, and focal neurological deficits. Clinical examination may reveal signs of raised intracranial pressure **(Furie & Provenzale, 1995).** The rise in incidence among children is partly attributed to improved diagnostic methods and increased awareness among physicians **(Fujimoto *et al*., 2000; Furie & Provenzale, 1995).**

2.6 The Role of Computed Tomography (CT) in Neuro-oncology

2.6.1 Technical Advantages and Historical Context

Developed in the mid-1970s, the CT scan revolutionized the diagnosis of brain tumors **(Dandy, 1918).** CT images provide detailed visualization of intracranial structures: the skull, blood clots, and calcified masses appear white; normal brain tissue appears gray; while cerebrospinal fluid (CSF), fat, and air appear black (**Silver *et al*., 1982; Dandy, 1918).** CT has the capacity to differentiate a wide range of tissue types—including air, fat, soft tissue,

and bone—with superior spatial resolution. The use of iodinated contrast agents allows for better delineation of vascular anatomy and pathological entities, helping to differentiate enhancing lesions from surrounding reactive changes. Furthermore, CT is highly sensitive to calcification and blood products within the brain parenchyma (**Silver *et al*., 1982).**

While Magnetic Resonance Imaging (MRI) is the gold standard for soft tissue characterization, CT offers unique advantages. It is highly sensitive to the detection of calcium, a key diagnostic feature for tumors such as craniopharyngiomas, oligodendrogliomas, and meningiomas (**Gomez *et al*., 2018).** Additionally, CT provides unparalleled detail of the skull base and calvarium, making it indispensable for evaluating bone destruction, remodeling, or hyperostosis (**Arora *et al*., 2022).**

2.6.2 Advantages in Specific Clinical Settings

CT is often preferred for uncooperative or unstable patients because each axial image is obtained separately. Consequently, motion artifact is minimized, particularly with later-generation scanners, which can perform individual scans in less than two seconds. This makes CT an invaluable tool in emergency and pediatric settings where patient cooperation may be limited **(Nelson *et al*., 1991).**

2.6.3 Contrast-Enhanced CT Imaging

To improve diagnostic accuracy, a contrast medium (CM) is often administered intravenously before the scan. This provides better detail and allows for superior visualization of the tumor's exact site, size, and borders. When the brain absorbs these contrast factors, most primary and secondary (malignant) tumors can be detected more clearly. Malignant neoplasms often show enhancement due to their unclear boundaries and abnormal blood vessels. After contrast administration, a tumor may appear either hypodense (showing low contrast uptake) or hyperdense (showing high contrast uptake), which helps in characterizing the lesion **(Bondy *et al*., 2008; Chang *et al*., 2007).**

2.6.4 CT Versus MRI

A CT scan may be used preferentially over MRI in specific clinical situations, such as when a patient has ferromagnetic materials or implants, or when there are other contraindications for undergoing an MRI scan. Therefore, CT remains an indispensable tool in neuro-oncology for both initial diagnosis and treatment planning (American Society of Clinical Oncology **[ASCO], 2022; Clarke, 2005).**

2.7 WHO 2021 Classification and its Radiological Implications

The fifth edition of the WHO Classification of CNS Tumors (2021) introduced a paradigm shift by integrating molecular and genetic markers into the diagnostic criteria (McNamara *et al*., 2022). This update has significant implications for radiologists, as imaging features are now being correlated with specific molecular signatures. For example, the presence of calcification in a frontal lobe mass may suggest an IDH-mutant, 1p/19q-codeleted oligodendroglioma **(Kurokawa *et al*., 2022).**

2.8 Multi-parametric CT Imaging Features of Brain and Skull Tumors

A multi-parametric approach to CT interpretation—incorporating density, enhancement patterns, necrosis, calcification, edema, and mass effect—is essential for narrowing the differential diagnosis.

2.8.1 Tumors Occurring in All Regions of the Skull Base

2.8.1.1 Meningioma

Meningiomas are extra-axial, dural-based tumors that arise from arachnoid cap cells. Although the majority are benign (World Health Organization [WHO] grade 1), they can present as atypical (grade 2) or, rarely, malignant (grade 3) variants. On non-contrast computed tomography (CT), meningiomas typically appear isodense to gray matter. On magnetic resonance imaging (MRI), they are generally isointense to slightly hyperintense relative to gray matter and demonstrate avid contrast enhancement; however, imaging

appearances can vary considerably due to the existence of multiple histological subtypes. Calcifications are observed in approximately 20–30% of cases **(Greenberg *et al*., 1999).**

A classic associated imaging feature is the "dural tail sign," which reflects reactive dural thickening and perilesional meningeal enhancement. This finding is present in 60–72% of meningiomas (Wallace, 2004). However, it is not entirely specific for meningioma, is less commonly observed in skull base locations, and may also be seen in other pathological processes such as lymphoma, tuberculosis, sarcoidosis, immunoglobulin G4-related disease, granulomatosis with polyangiitis, and fungal infections **(Wallace, 2004; Matias *et al*., 2023).**

Meningiomas that abut the skull base are frequently associated with focal hyperostosis of the adjacent bone. The exact pathogenesis of this hyperostosis remains incompletely understood, but it is thought to result from osteoblastic stimulating factors, direct tumoral invasion, or a combination of both mechanisms (Casselman *et al*., 2019). Additionally, enlargement of adjacent paranasal sinuses, particularly pneumosinus dilatans (upward blistering of the sphenoid sinus), has been associated with anterior cranial fossa meningiomas, especially those arising along the planum sphenoidale.

Petroclival and parasellar meningiomas tend to involve critical neurovascular structures, including the cavernous sinus, optic canal, and Meckel's cave. A useful distinguishing feature from pituitary adenomas is the narrowing of encased arteries, which is typically seen in meningiomas but not in pituitary adenomas **(see Figure 1) (Zamora & Castillo, 2017).**

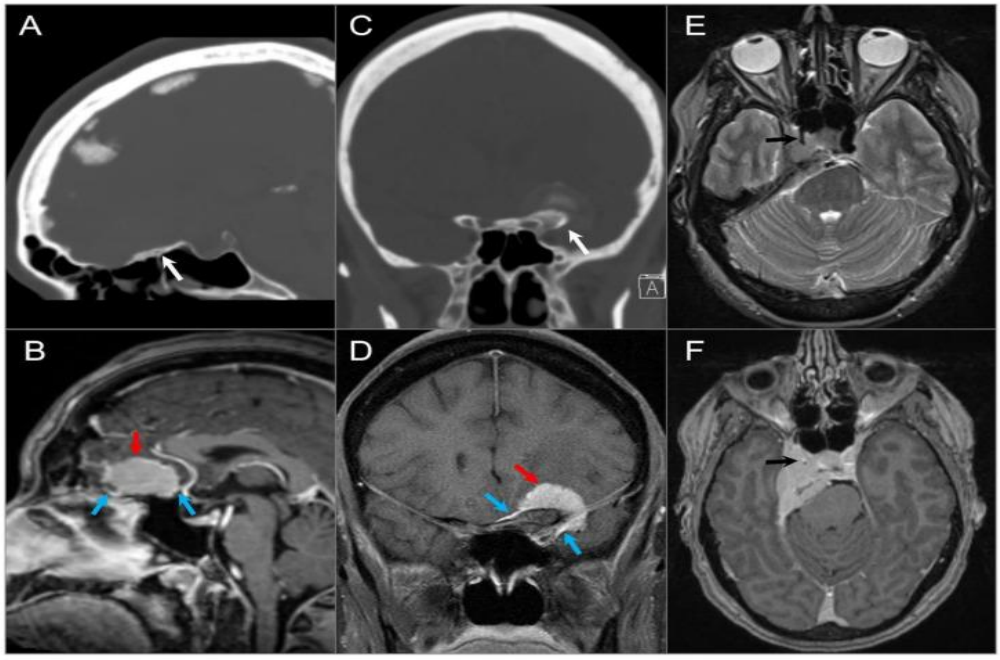

(Zamora & Castillo, 2017).

Figure 1 Meningiomas in three different patients. (A) Sagittal CT and (B) sagittal postcontrast T1W MR images demonstrate a homogenously enhancing extra-axial mass lesion (red arrow) at the anterior cranial fossa/planum sphenoidale with small dural tails (blue arrows) and hyperostosis (white arrow). (C) Coronal CT and (D) coronal postcontrast fat-saturated T1W images show an anterior clinoid process meningioma (red arrow) with dural tails (blue arrows), hyperostosis (white arrow), and tumoral calcification. (E) Axial T2W and (F) axial postcontrast T1W images reveal a right cavernous sinus meningioma extending through the petroclival dura, tentorium, and paraclinoid dura. The mass completely encases the right ICA with significant narrowing (black arrows).

En plaque meningiomas are characterized by sheet-like dural thickening rather than a globular mass, and they are associated with more prominent subjacent hyperostosis. The distinction between an en plaque meningioma with a significant osseous component and a primary intraosseous meningioma is often vague and relatively arbitrary **(see Figure 2).**

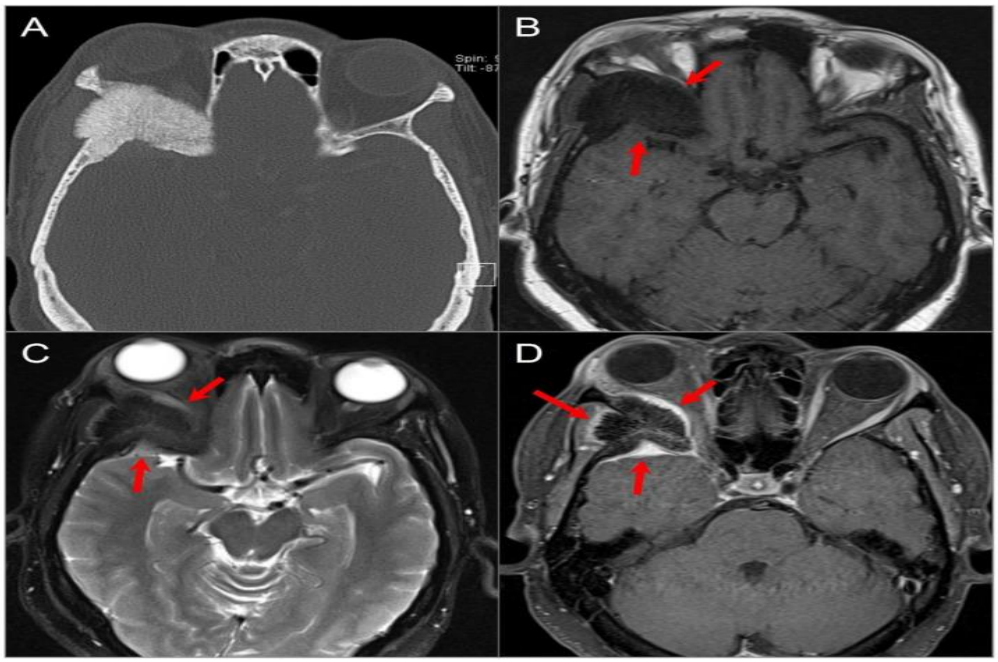

Figure 2 Intraosseous meningioma. (A) Axial CT shows a marked osseous expansion of the right posterolateral orbital wall and a greater wing of the sphenoid with a spiculated appearance. (B) Axial T1W and (C) STIR T2W images show marked hypointensity in the lesion with thin surrounding soft tissue components along the lateral orbital wall and temporal fossa (arrows). (D) Axial fat-suppressed postcontrast T1W image demonstrates heterogenous transosseous enhancement and avid contrast enhancement in the soft tissue components of the lesion along the temporal dura and orbital/temporal periosteum (red arrows). There is associated displacement of extraocular muscles and proptosis. (Casselman *et al*., 2019).

Higher-grade (atypical or malignant) meningiomas may demonstrate lytic and destructive bony features. In such cases, alternative pathologies such as solitary fibrous tumor or metastasis should be considered in the differential diagnosis.

While MR spectroscopy is not routinely used for diagnosis, it may provide adjunctive information in equivocal cases. Short echo time (TE) proton (^{1}H) MR spectroscopy may reveal an alanine peak at 1.3–1.5 parts per million (ppm) and increased glutamine and glutamate peaks, which can be helpful in supporting the diagnosis of meningioma (Casselman *et al*., 2019).

2.8.1.2 Schwannoma

Schwannomas are benign, slow-growing neoplasms that arise from Schwann cells and can involve cranial nerves (CNs) III through XII in the central and posterior skull base. Although olfactory nerves lack Schwann cells and are thus typically spared, schwannomas arising from the olfactory filia directly below the cribriform plate have been reported but are extremely rare (Skolnik *et al*., 2016).

Schwannomas account for approximately 8.5% of all intracranial tumors and are usually diagnosed in adulthood (Zamora & Castillo, 2017). The majority of intracranial schwannomas originate from CN VIII, primarily involving the cerebellopontine angle (CPA) cistern (90%), followed by CN V (1–8%) and CN VII (Chowdhury *et al*., 2014). Intraorbital schwannomas commonly arise from the supraorbital and supratrochlear nerves in the upper orbital cavity. In the central parasellar skull base, CN V schwannomas predominate, while schwannomas involving CN III, IV, and VI are rare, except in the setting of neurofibromatosis type 2 (NF2)-related schwannomatosis (Chowdhury *et al*., 2014).

Vestibular schwannomas are the most frequent form of posterior skull base schwannomas, accounting for 85% of all CPA masses and 6–10% of all intracranial tumors (Moffat & Ballagh, 1995; Farid, 2014). Schwannomas of CN X, and especially those of CNs IX, XI, and XII, are rare. The majority of schwannomas are slow-growing, with an estimated progression rate of 1–2 mm per year (Nikolopoulos *et al*., 2010).

On magnetic resonance imaging (MRI), schwannomas appear as well-circumscribed, round or lobulated masses. They are generally solid, demonstrating T1 isointensity and T2 hyperintensity relative to gray matter, and show avid contrast enhancement. A classic "ice cream on cone" appearance is typical for vestibular schwannomas involving the CPA, although small lesions may be purely intracanalicular. Schwannomas may demonstrate varying degrees of heterogeneity due to cystic change or, rarely, hemorrhage or calcification (MacNally *et al*., 2008; Zhang *et al*., 2009; Liu *et al*., 2009). This variability is illustrated in **Figure 3.**

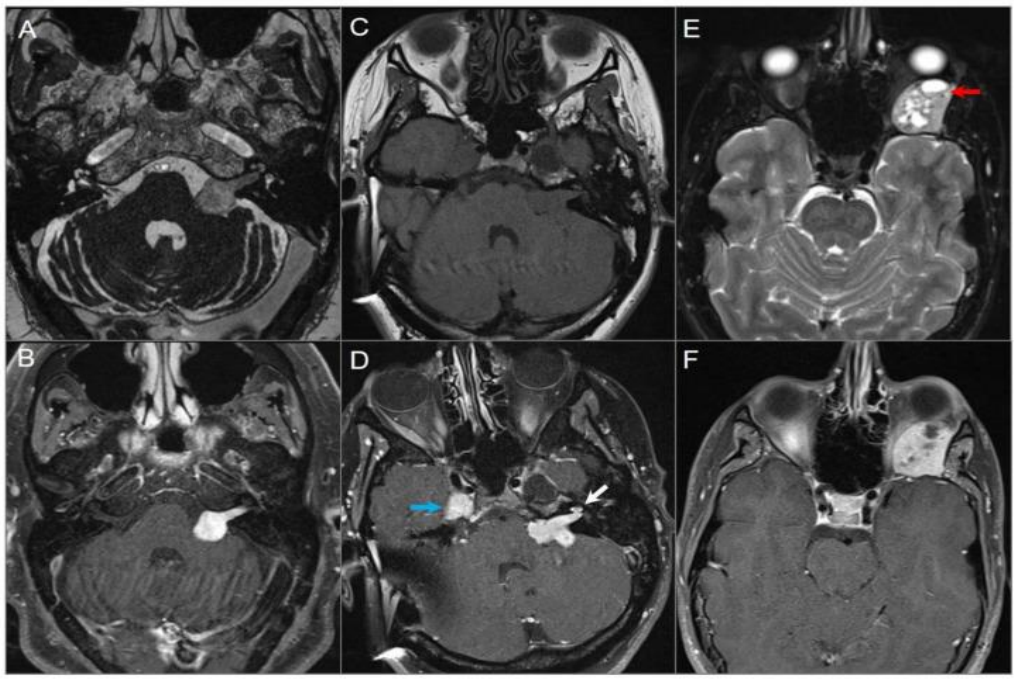

Figure 3. Schwannomas in three different patients. (A) Axial CISS and (B) axial postcontrast fat-suppressed T1W images show a well-defined, homogenously enhancing left CPA mass with extension into the left internal auditory canal. (C) Axial T1W and (D) postcontrast axial fat-suppressed T1W images show multiple schwannomas centered in the right Meckel's cave (blue arrow) and the left CPA in a patients with NF2-related schwannomatosis. The left CPA mass completely fills the IAC and extends into the cochlea (white arrow). (E) Axial T2W and (F) axial postcontrast fat-suppressed T1W images reveal a left orbital extraconal, well-defined, heterogeneously enhancing intra-orbital schwannoma with bone remodeling/dehiscence and mass effect on the optic nerve and extraocular muscles. The mass contains multiple non enhancing areas of cystic degeneration with fluid–fluid levels likely due to hemorrhage (red arrow). **(MacNally *et al*., 2008; Zhang *et al*., 2009; Liu *et al*., 2009).**

Melanotic schwannomas are a rare variant and exhibit intrinsic T1 hyperintensity due to melanin content. This finding can lead to confusion with lipomas; however, the use of fat-saturated MRI sequences can aid in distinguishing between the two entities (Buhl *et al*., 2004; Dahlen *et al*., 2002).

2.8.1.3 Metastasis

Skull base metastases occur in approximately 4% of cancer patients and are generally associated with advanced disease. They are most frequently found in the clivus, petrous apex, and sphenoid bone, likely due to the higher marrow content in these regions. Although various primary tumors may give rise to skull base metastases, the most common origins are breast, prostate, and lung carcinomas, as well as lymphoma (Zamora & Castillo, 2017; Laigle-Donadey *et al*., 2005).

Hematogenous spread is the most common mechanism for metastatic dissemination. However, other pathways include seeding through the valveless Batson venous plexus, direct extension from sinonasal, nasopharyngeal, or sphenoid tumors, and perineural spread, which commonly occurs along branches of CN V (Zamora & Castillo, 2017; Laigle-Donadey *et al*., 2005).

Skull base metastases are often clinically silent until there is involvement of cranial nerves, which can lead to specific neuropathies. Among these, CN VI palsy is the most frequently observed neurological deficit. The imaging appearance can be variable depending on the histology of the primary tumor. On computed tomography (CT), lesions may have a lytic or sclerotic appearance. On MRI, most lesions show T1 hypointense signals due to the replacement of the normally hyperintense fatty marrow, as well as contrast enhancement. T2 signal changes and contrast enhancement are best appreciated on fat-saturated sequences. Additionally, diffusion-weighted imaging (DWI) sequences can be helpful in demonstrating bony metastases, as they are frequently associated with restricted diffusion **(see Figure 4).**

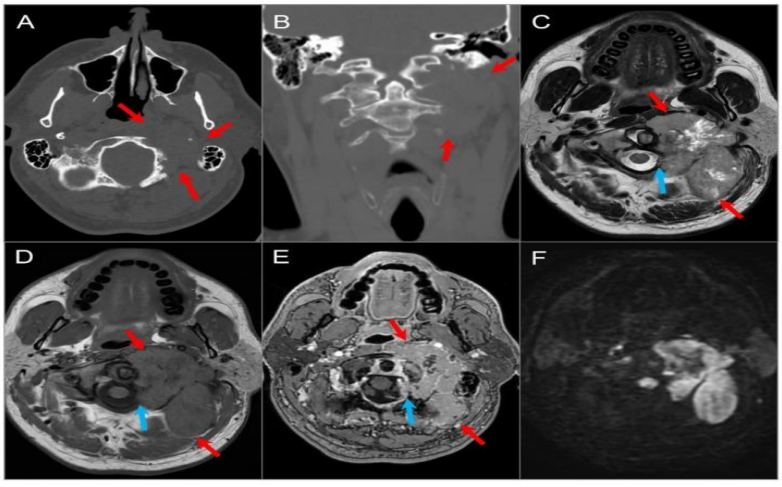

Figure 4 Skull base metastasis from RCC. (A) Axial and (B) coronal CT images show a lucent destructive soft tissue density mass lesion (red arrows) involving the left occipital bone, including occipital condyle, left lateral mass of C1, and inferomedial mastoid. (C) T2W, (D) noncontrast T1W, and (E) postcontrast T1W images reveal a bulky mass (red arrows) involving the left skull base and extending to the left retropharyngeal region and left epidural space (blue arrows). The lesion shows avid enhancement with central cystic/necrotic degeneration. (F) DWI image shows hyperintense signal in the solid components of the lesion consistent with restricted diffusion due to high cellularity.

2.8.1.4 Fibrous Dysplasia

Fibrous dysplasia is a developmental fibro-osseous disorder characterized by defective osteoblastic differentiation and maturation. This process results in the replacement of mature lamellar bone with fibrous tissue and immature woven bone. It is not considered a true neoplasm but is classified as a benign bony tumor in the World Health Organization (WHO) classification (fifth edition) (WHO Classification of Tumours Editorial Board, 2020).

Fibrous dysplasia can affect any bone, including those of the skull base, and may occur in a monostotic (involving a single bone) or polyostotic (involving multiple bones) form. Lesions can exhibit varying and heterogeneous internal architecture, which can result in diverse imaging appearances on CT and, particularly, MRI (Kushchayeva *et al*., 2018; Casselman *et al*., 1993).

CT is the preferred imaging modality for diagnosing fibrous dysplasia. It typically shows an expansile, homogeneously sclerotic bone lesion with a characteristic ground-glass appearance. However, MRI findings can be difficult to interpret due to variations in bony trabecular composition, cellularity, collagen content, and the presence of cystic and hemorrhagic degeneration. These factors contribute to signal heterogeneity and may mimic a malignant or aggressive lesion **(see Figure 5) (Kushchayeva *et al*., 2018; Casselman *et al*., 1993).**

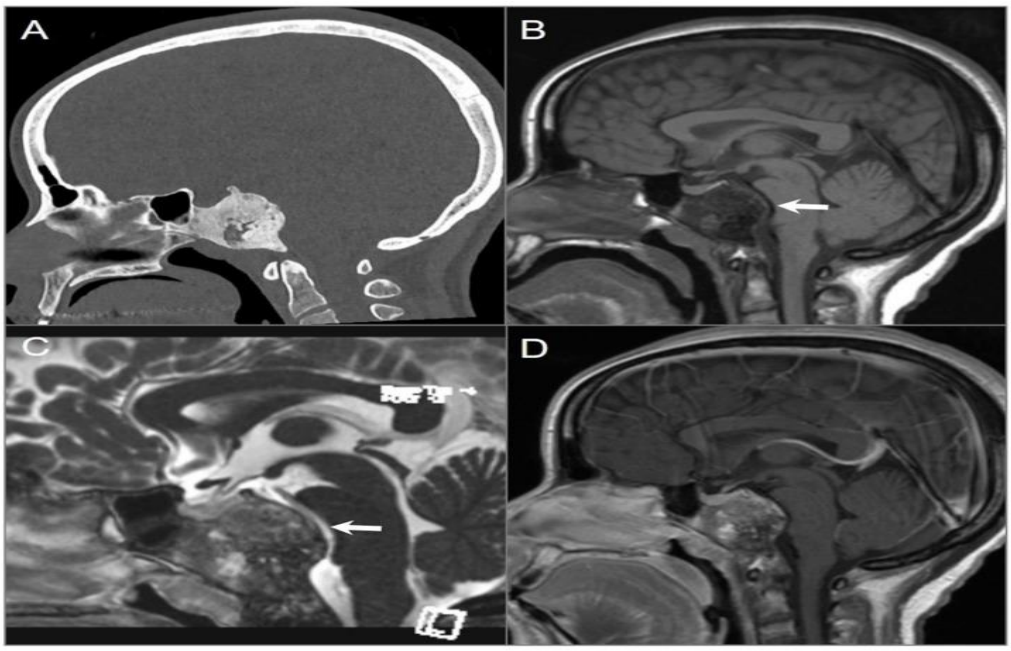

Figure5 Fibrous dysplasia. (A) Sagittal CT image shows a well-defined expansile ground-glass density lesion in the clivus and posterior sphenoid sinuses. The lesion demonstrates peripheral sclerotic and central small lytic regions. (B,C) Sagittal T1W and postcontrast CISS images reveal T1 hypointense and variable T2 signal intensity in the lesion with mass effect on the brainstem and basilar artery (arrows). (D) Sagittal postcontrast T1-weighted image shows heterogeneous enhancement of the lesion.

On fluorodeoxyglucose-positron emission tomography (FDG-PET) CT, the lesions show variable and sometimes intense FDG uptake, which may be misinterpreted as metastases or a malignant tumor (Iida & Anzai, 2017).

2.8.2 Posterior Skull Base and Jugular Foramen Lesions

2.8.2.1 Paraganglioma

Glomus jugulare and glomus tympanicum, also known as paragangliomas, are tumors that develop from glomus bodies near Jacobson's nerve (the tympanic branch of cranial nerve IX) and Arnold's nerve (the auricular branch of cranial nerve X). They typically affect adults aged between 40 and 60 years and are more common in women (Casselman *et al*., 2019; Rao *et al*., 1999). Patients may present with an isolated primary jugular fossa paraganglioma

(glomus jugulare) or with a tumor that extends to the middle ear along Jacobson's nerve, referred to as glomus jugulotympanicum. Glomus tympanicum classically arises from the cochlear promontory and can be seen as a small red mass in the anterior inferior quadrant of the tympanic membrane during otoscopy. Up to 10% of patients may have multiple paragangliomas, particularly when occurring in association with succinate dehydrogenase gene mutations (Casselman *et al*., 2019; Vogl & Bisdas, 2009).

The clinical presentation varies depending on the degree of involvement of the jugular fossa and middle ear, and may include symptoms such as pulsatile tinnitus, hearing loss, and cranial nerve palsies. Assessing the extent of bony erosion, involvement of the middle ear cavity, and intracranial extension is critical for surgical planning. Computed tomography (CT) is the modality of choice to demonstrate erosion of adjacent bony structures, including the jugular and caroticojugular spines. CT is also helpful for determining the degree of extension into the middle ear cavity and infratemporal fossa, as well as the integrity of the ossicles and bony labyrinth (Rao *et al*., 1999; Tuan *et al*., 2014; Rigby & Jackler, 1996).

These tumors are highly vascular and can be assessed with digital subtraction angiography (DSA) and magnetic resonance angiography (MRA), which reveal an intense tumor blush, feeding vessels primarily from the ascending pharyngeal artery, and early venous drainage due to intratumoral shunts. On magnetic resonance imaging (MRI), a "salt and pepper" appearance can be seen on T1-weighted and T2-weighted images, where the "salt" represents blood products from hemorrhage or slow flow and the "pepper" represents flow voids due to high vascularity. Intense enhancement is typical on both CT and MRI **(Figure 6) (Rao *et al*., 1999; Rigby & Jackler, 1996).** Surgery is the primary treatment, but large inoperable tumors or those in poor surgical candidates can be treated with radiotherapy, as these lesions are radiosensitive (Casselman *et al*., 2019; Vogl & Bisdas, 2009).

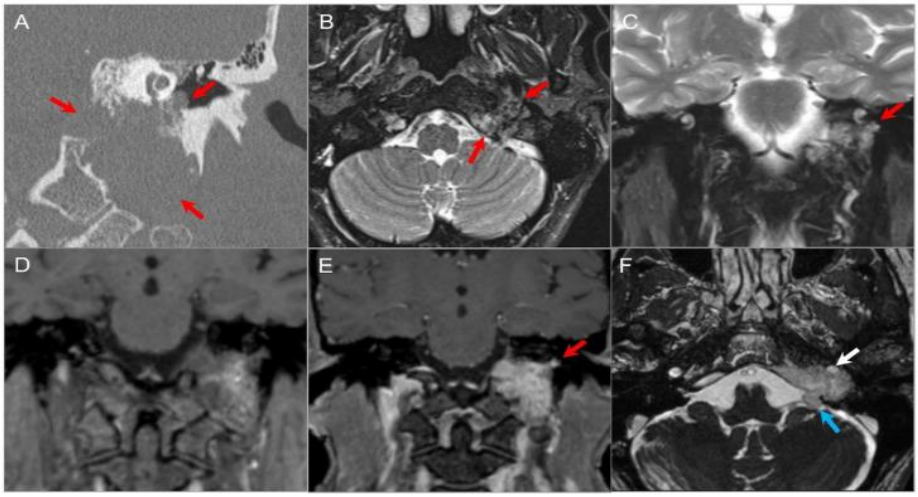

Figure 6 Glomus jugulotympanicum. (A) Coronal CT image demonstrates a soft tissue density lesion in the left jugular fossa with irregular moth-eaten osseous erosion. The mass extends into the middle ear cavity at the cochlear promontory (red arrows), confirming a combined glomus jugulotympanicum. (B) Axial and (C) coronal fat-suppressed T2W images demonstrate heterogeneous hyperintense signal in the lesion (red arrows) with tiny signal voids consistent with hypervascularity. (D) Coronal noncontrast T1W image demonstrates a 'salt and pepper' appearance with small foci of hyper- and hypointensity. (E) Coronal postcontrast T1W image shows avid enhancement of the lesion (red arrow). (F) Axial postcontrast CISS image reveals partial encasement of the left ICA (white arrow) and polypoid extension of the lesion into the left CPA cistern (blue arrow) due to dural disruption (Rao *et al*., 1999; Rigby & Jackler, 1996).

2.8.3 Primary Brain Lymphoma

Primary brain lymphoma is a relatively rare CNS malignancy, accounting for approximately 1.5% of all intracranial tumors (Dolecek *et al*., 2012). However, its incidence is increasing due to immunocompromised states from widespread use of immunological agents and organ transplantation (Korfel *et al*., 2015; Hoang-Xuan *et al*., 2015). The universal principle for treating intracranial tumors is "early detection and early treatment." However, primary brain lymphoma shows no obvious signs during early stages, and specific imaging features are often lacking, making early diagnosis difficult (Touitou *et al*., 2015;

Houillier *et al*., 2015). Therefore, studies aim to analyze the specific CT features that may aid in the early detection of this malignancy (Touitou *et al*., 2015).

2.9 Diagnostic Performance and Histopathological Correlation

The diagnostic performance of CT in neuro-oncology is measured by its sensitivity and specificity. While CT has high sensitivity for detecting intracranial masses, its specificity for determining the exact histological type can be limited compared to MRI. However, when multi-parametric features are combined with demographic data, diagnostic accuracy improves significantly (JDPO, 2023). Histopathological examination remains the reference standard, and the correlation between radiological features and pathological findings is crucial for refining diagnostic algorithms. Studies have shown that certain CT signatures, such as the combination of hyperdensity and intense enhancement in meningiomas, have a high positive predictive value **(New *et al*., 1980).**

Chapter Three

Methodology

3. Methodology

3.1 Study Design and Setting

This study was designed as a descriptive cross-sectional study conducted at the National Oncology Center (NOC), Sana'a, Yemen, which is the leading tertiary referral center for oncology cases in the country. The study protocol was reviewed and approved by the Institutional Review Board (IRB) of the National Oncology Center (Reference No.: NOC-IRB-2024-07).

Patient confidentiality was strictly maintained through complete anonymization of all extracted data. Because the study was retrospective and based on previously recorded clinical and radiological data, the requirement for individual informed consent was waived by the IRB.

3.2 Study Duration

The study was conducted over a five-month period from October 2025 to February 2026. Data included patients examined between August 2024 and November 2025.

3.3 Study Population

The study population consisted of patients aged 2 to 75 years with a confirmed diagnosis of brain or skull tumors (primary or metastatic) who underwent contrast-enhanced CT imaging of the brain and/or head and neck at the National Oncology Center.

3.4 Sample Size and Sampling Technique

A total of 52 consecutive patients meeting the eligibility criteria were included in this study. A consecutive sampling technique was used to include all eligible patients within the specified study period.

3.5 Eligibility Criteria

3.5.1 Inclusion Criteria

Patients were included if they met the following criteria:

- Confirmed diagnosis of brain or skull tumor (primary or metastatic).
- Availability of complete contrast-enhanced CT imaging studies.
- Availability of comprehensive clinical and demographic data.
- Imaging performed between August 2024 and November 2025.

3.5.2 Exclusion Criteria

Patients were excluded if they had:

- Incomplete or poor-quality imaging studies.
- Non-neoplastic lesions (e.g., cysts or inflammatory processes).
- Insufficient clinical documentation.

3.6 Study Variables

The study variables were categorized as follows:

3.6.1 Demographic Variables

- Age
- Gender

3.6.2 Tumor Characteristics

Tumor category (Primary CNS, Metastatic, Paraganglioma, Hematologic, Orbital, Vascular)

Tumor subcategory

Location (Cerebral, Cerebellar, Skull, Extra-axial, Orbit, CPA, Posterior Fossa, Multiple)

Multiplicity (Solitary, Few [2–4], Multiple)

3.6.3 CT Imaging Features

Density (Hypodense, Iso-dense, Hyperdense, Mixed, Lytic)

Enhancement pattern (None, Mild, Moderate, Strong)

Secondary CT features:

Necrosis (Yes/No)

Calcification (Yes/No)

Edema (Yes/No)

Mass effect (Yes/No)

3.7 Imaging Equipment

CT examinations were performed using a 64-slice multidetector computed tomography scanner (Philips CT System, manufactured July 2012, installed 2016) located in the CT Scan Department at the National Oncology Center.

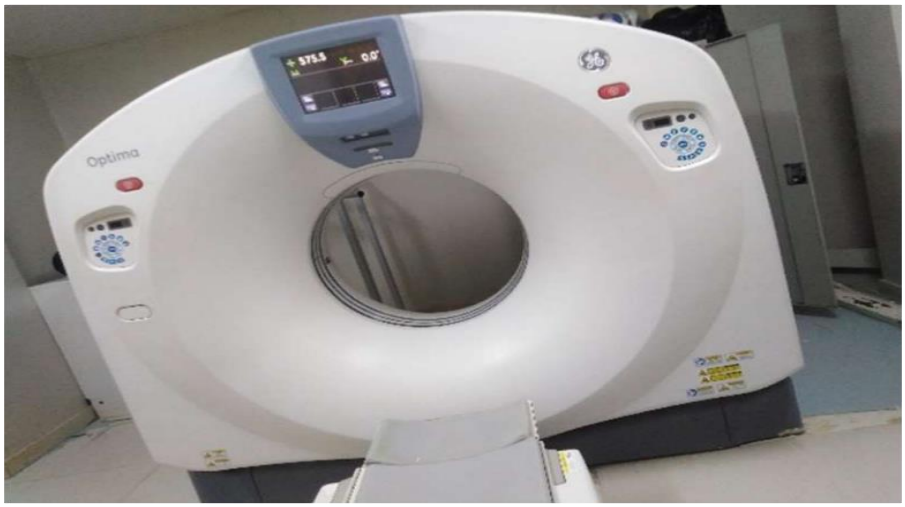

Figure (3.1) CT scan unit

3.8 CT Imaging Protocol

3.8.1 Non-Contrast CT Parameters

Scan range: From foramen magnum to vertex

Slice thickness: 0.625 mm (acquisition), reconstructed at 1 mm and 3 mm

Tube voltage: 120 kVp

Tube current: Automatic dose modulation

Rotation time: 0.5 seconds

Pitch: 0.8

Reconstruction kernel: Standard brain algorithm

Matrix: 512 × 512

3.8.2 Contrast-Enhanced CT Parameters

Contrast agent: Iohexol (Omnipaque 350)

Dosage: 1.5 mL/kg body weight (maximum 100 mL)

Injection rate: 3 mL/second using a power injector

Scan delay: 60 seconds post-injection

Imaging parameters identical to non-contrast acquisition

3.11 Data Collection and Management

Clinical and radiological data were extracted retrospectively from medical records and radiology reports. Data were recorded using structured data collection sheets and subsequently entered into Microsoft Excel for coding and verification.

All data were anonymized prior to statistical analysis.

3.12 Statistical Analysis

Statistical analysis was performed using SPSS version 23.0. All tests were two-tailed, and statistical significance was set at $p < 0.05$.

3.12.1 Descriptive Statistics

Continuous variables were expressed as mean ± standard deviation.

Categorical variables were expressed as frequencies and percentages.

3.12.2 Inferential Statistics

Chi-square test or Fisher's exact test was used for categorical variables.

Independent sample t-test or one-way ANOVA was used for continuous variables, where appropriate.

Inter-observer agreement was assessed using Cohen's kappa coefficient (κ).

3.10. Ethical Considerations:

- The study adhered to the ethical standards of the 21 September University.
- Patient confidentiality was ensured by anonymizing all medical records and imaging data. No personal identifiers were included in the data analysis process..
- Ethical approval was obtained from the Institutional Review Board of the National Oncology Center. The study adhered to the principles of the Declaration of Helsinki.
- Radiation exposure was conducted according to institutional safety protocols following the ALARA (As Low As Reasonably Achievable) principle.

Chapter Four

Results

and

Discussion

4.1 Results

4.1 Demographic Characteristics

This section details the demographic profile of the study cohort, specifically focusing on age distribution and gender ratio, thereby addressing the first specific research objective.

Table 4.1: Demographic Characteristics of the Study Cohort (N=52)

Variable	Overall (N=52)	Primary CNS (n=21)	Metastatic (n=24)	Paraganglioma (n=3)	Hematologic (n=1)	Orbital (n=3)	p-value
Age, years							
Mean ± SD	45.2 ± 19.8	40.1 ± 20.3	50.8 ± 17.9	32.7 ± 21.0	38	35.0 ± 31.2	0.001*
Range	2–73	2–73	18–79	18–60	38	2–65	
Age Groups							
≤18 years	8 (15.4%)	5 (23.8%)	2 (8.3%)	1 (33.3%)	0	0	0.012*
19–40 years	16 (30.8%)	6 (28.6%)	7 (29.2%)	1 (33.3%)	1 (100%)	1 (33.3%)	
41–60 years	17 (32.7%)	6 (28.6%)	9 (37.5%)	1 (33.3%)	0	1 (33.3%)	
>60 years	11 (21.2%)	4 (19.0%)	6 (25.0%)	0	0	1 (33.3%)	
Gender							
Male	18 (34.6%)	7 (33.3%)	7 (29.2%)	3 (100%)	0	1 (33.3%)	0.045*
Female	34 (65.4%)	14 (66.7%)	17 (70.8%)	0	1 (100%)	2 (66.7%)	

Table 4.1: The demographic analysis of the study cohort (N=52) revealed significant variations across different tumor categories. The mean age of patients significantly differed among tumor types (p=0.001), with metastatic tumors presenting in older individuals (mean age 50.8 ± 17.9 years) compared to primary Central Nervous System (CNS) tumors (40.1 ± 20.3 years). The age group of 41–60 years constituted the largest proportion of the overall cohort (32.7%). Primary CNS tumors were more frequently observed in younger patients (≤18 years: 23.8%), whereas metastatic tumors were more prevalent in older age groups (>40 years). Gender distribution also exhibited a significant association with tumor type (p=0.045). Overall, there was a female predominance (65.4%), which was consistent across most tumor categories. However, all paraganglioma cases in this cohort were exclusively male. These findings comprehensively address the first research objective concerning the demographic composition of patients with brain and skull tumors.

4.2 Tumor Categories and Scientific Classification

This section presents an analysis of the frequency and scientific subtypes of the identified tumor categories, addressing the second research objective.

Table 4.2: Tumor Category and Scientific Subtype Distribution (N=52)

Tumor Category	Scientific Subtype	n (%)	Mean Age	Gender (F:M)	Key CT Feature
Primary CNS		**21 (40.4%)**	**40.1**	**14:07**	
	Gliomas/Astrocytomas	5 (9.6%)	46	3:02	Hypodense + Edema
	Meningiomas	4 (7.7%)	49	3:01	Hyperdense + Calcification
	Medulloblastoma	1 (1.9%)	52	1:00	Hyperdense, Cystic
	PFT	1 (1.9%)	7	1:00	Mixed, Cystic
	Other Primary CNS	10 (19.2%)	36.5	6:04	Variable
Metastatic		**24 (46.2%)**	**50.8**	**17:07**	
	Breast Cancer	9 (17.3%)	48.3	9:00	Strong enhancement + Necrosis
	Nasopharyngeal CA	5 (9.6%)	44	3:02	Iso/Mixed density
	Skin Cancer (SCC)	4 (7.7%)	50.3	4:00	Mixed, Lytic
	Prostate Cancer	1 (1.9%)	61	0:01	Mixed, Calcified
	Lung Cancer	1 (1.9%)	37	1:00	Hypodense

Tumor Category	Scientific Subtype	n (%)	Mean Age	Gender (F:M)	Key CT Feature
	Other Metastases	4 (7.7%)	33.6	0:04	Variable
Paraganglioma	Glomus Tumors	3 (5.8%)	32.7	0:03	Iso-dense + Calcification
Hematologic	Lymphoma	1 (1.9%)	38	1:00	Iso-dense, Strong enhancement
Orbital	Orbital Tumors	3 (5.8%)	35	2:01	Iso-dense, Moderate enhancement
Total		**52 (100%)**	**45.2**	**34:18**	

Table 4.2: Metastatic tumors represented the most frequent category in the cohort, accounting for 46.2% (n=24) of all cases, closely followed by primary CNS tumors at 40.4% (n=21). Within the primary CNS group, gliomas/astrocytomas (9.6%, n=5) and meningiomas (7.7%, n=4) were the most commonly identified subtypes. Among metastatic tumors, breast cancer metastases were predominant, constituting 17.3% (n=9) of the total cohort, which aligns with the observed female predominance in the study. Paraganglioma, hematologic, and orbital tumors comprised smaller proportions of the cohort, at 5.8% (n=3), 1.9% (n=1), and 5.8% (n=3), respectively. This detailed classification addresses the second research objective by providing a comprehensive overview of tumor categories and their scientific subtypes within the study population.

4.3 Anatomical Location Analysis

This section investigates the topographic distribution of tumors, contributing to the general objective of evaluating their anatomical features.

Table 4.3: Anatomical Location Distribution by Tumor Category

Location	Overall (N=52)	Metastatic Only (n=24)	Non-Metastatic (n=28)
Cerebral	25 (48.1%)	12 (50.0%)	13 (46.4%)
Cerebellar	14 (26.9%)	7 (29.2%)	7 (25.0%)
Skull	18 (34.6%)	10 (41.7%)	8 (28.6%)
Extra-axial	5 (9.6%)	1 (4.2%)	4 (14.3%)
Orbit	3 (5.8%)	0	3 (10.7%)
CPA	3 (5.8%)	2 (8.3%)	1 (3.6%)
Scalp	4 (7.7%)	0	4 (14.3%)
Posterior Fossa	2 (3.8%)	0	2 (7.1%)
Multiple Locations	18 (34.6%)	11 (45.8%)	7 (25.0%)

Table 4.3: The analysis of anatomical distribution revealed that the cerebral region was the most common tumor location overall, observed in 48.1% (n=25) of cases. This was followed by the skull (34.6%, n=18) and the cerebellar region (26.9%, n=14). A notable difference was observed in skull involvement, which was higher in metastatic tumors (41.7%) compared to non-metastatic tumors (28.6%). Conversely, orbital and scalp locations were exclusively associated with non-metastatic tumors, suggesting these sites might be characteristic of primary lesions. Furthermore, multiple location involvement was significantly more frequent in metastatic tumors (45.8%) than in non-metastatic tumors (25.0%), which supports the multifocal nature often associated with metastatic disease. These findings contribute to understanding the topographic features of brain and skull tumors.

4.4 Lesion Multiplicity Patterns

This section assesses the patterns of lesion multiplicity across different tumor categories, addressing the fourth specific research objective.

Table 4.4: Lesion Multiplicity by Tumor Type

Multiplicity	Overall (N=52)	Primary CNS (n=21)	Metastatic (n=24)	Paraganglioma (n=3)	Hematologic (n=1)	Orbital (n=3)
Solitary	33 (63.5%)	15 (71.4%)	11 (45.8%)	3 (100%)	1 (100%)	3 (100%)
Multiple	19 (36.5%)	6 (28.6%)	13 (54.2%)	0	0	0

*Statistical Significance: $\chi^2 = 15.23$, $p = 0.002$

Table 4.4: Lesion multiplicity analysis demonstrated a statistically significant association with tumor type ($\chi^2 = 15.23$, $p = 0.002$). Metastatic tumors were significantly more prone to presenting as multiple lesions (54.2%) compared to primary CNS tumors (28.6%). Notably, all cases of paraganglioma, hematologic, and orbital tumors were solitary. This finding is consistent with the established understanding that the presence of multiple lesions is a characteristic feature often indicative of metastatic disease. The statistically significant association observed underscores the diagnostic utility of lesion multiplicity in differentiating between various tumor types.

4.5 CT Imaging Characteristics

This section analyzes the frequency of specific CT imaging features across different tumor categories, addressing the second specific research objective related to imaging characteristics.

Table 4.5: CT Density and Enhancement Patterns by Tumor Type

CT Feature	Overall (N=52)	Primary CNS (n=21)	Metastatic (n=24)	Paraganglioma (n=3)	Hematologic (n=1)	Orbital (n=3)
Density						
Hypodense	19 (36.5%)	8 (38.1%)	10 (41.7%)	0	0	1 (33.3%)
Iso-dense	19 (36.5%)	6 (28.6%)	6 (25.0%)	3 (100%)	1 (100%)	3 (100%)
Hyperdense	7 (13.5%)	5 (23.8%)	1 (4.2%)	0	0	0
Mixed	15 (28.8%)	4 (19.0%)	9 (37.5%)	0	0	0
Lytic	2 (3.8%)	0	2 (8.3%)	0	0	0
Enhancement						
None	8 (15.4%)	3 (14.3%)	4 (16.7%)	0	0	1 (33.3%)
Mild	6 (11.5%)	2 (9.5%)	3 (12.5%)	0	0	1 (33.3%)
Moderate	14 (26.9%)	4 (19.0%)	6 (25.0%)	0	0	3 (100%)
Strong	24 (46.2%)	12 (57.1%)	11 (45.8%)	3 (100%)	1 (100%)	0
Associated Features						
Necrosis	31 (59.6%)	13 (61.9%)	17 (70.8%)	1 (33.3%)	0	0
Calcification	17 (32.7%)	9 (42.9%)	5 (20.8%)	3 (100%)	0	0

CT Feature	Overall (N=52)	Primary CNS (n=21)	Metastatic (n=24)	Paraganglioma (n=3)	Hematologic (n=1)	Orbital (n=3)
Edema	32 (61.5%)	14 (66.7%)	16 (66.7%)	0	1 (100%)	1 (33.3%)
Mass Effect	39 (75.0%)	16 (76.2%)	20 (83.3%)	3 (100%)	1 (100%)	0

Table 4.5: The analysis of CT imaging characteristics revealed distinct patterns across tumor types. Hypodense and iso-dense lesions were the most prevalent density patterns overall, each accounting for 36.5% of cases. Iso-dense lesions were particularly characteristic of paraganglioma (100%), hematologic (100%), and orbital tumors (100%). Strong enhancement was frequently observed in paraganglioma (100%) and hematologic tumors (100%), followed by primary CNS tumors (57.1%). Necrosis was most commonly associated with metastatic tumors (70.8%), while calcification was a hallmark feature of paraganglioma (100%) and primary CNS tumors (42.9%). Edema and mass effect were common findings across most categories; however, mass effect was notably absent in orbital tumors. These findings provide a detailed understanding of the frequency of specific CT features, addressing the second research objective.

4.6 Correlation Analysis: CT Features and Tumor Types

This section identifies statistically significant associations between CT feature patterns and specific tumor subcategories, addressing the third specific research objective.

Table 4.6: Correlation Matrix - Tumor Types vs. CT Features

CT Feature	Primary CNS	Metastatic	Paraganglioma	Hematologic	Orbital	Overall Correlation (r)
Hypodensity	0.12	0.18	-0.25	-0.15	0.08	0.21
Iso-density	-0.15	-0.22	0.68*	0.23	0.72*	0.35
Hyperdensity	0.42*	-0.31	-0.18	-0.12	-0.15	0.28
Strong Enhancement	0.25	0.18	0.65*	0.35	-0.52	0.38*
Necrosis	0.18	0.45*	-0.28	-0.35	-0.48	0.32
Calcification	0.35	-0.22	0.82**	-0.18	-0.25	0.41*
Edema	0.28	0.31	-0.42	0.35	-0.28	0.29
Mass Effect	0.22	0.38	0.45	0.28	-0.65	0.34

$p < 0.05$; $p < 0.01$

Table 4.6: Correlation analysis revealed several statistically significant associations between specific tumor types and CT features. Paraganglioma exhibited strong positive correlations with iso-density ($r=0.68$, $p<0.05$), strong enhancement ($r=0.65$, $p<0.05$), and calcification ($r=0.82$, $p<0.01$). Orbital tumors also showed a significant positive correlation with iso-density ($r=0.72$, $p<0.05$). Primary CNS tumors demonstrated a moderate positive correlation with hyperdensity ($r=0.42$, $p<0.05$), while metastatic tumors were significantly correlated with the presence of necrosis ($r=0.45$, $p<0.05$). These findings are crucial for

addressing the third research objective, as they identify specific CT imaging patterns that are significantly associated with particular tumor types.

Table 4.7: Scientific Subtype Correlations with Key CT Features

Tumor Subtype	Most Correlated CT Features	Correlation Coefficient (r)	p-value
Metastatic Breast	Strong enhancement + Necrosis	0.72	<0.001
Primary Gliomas	Hypodense + Edema	0.65	0.003
Meningiomas	Hyperdense + Calcification	0.81	<0.001
Paraganglioma	Iso-dense + Calcification	0.82	<0.001
Metastatic Skin	Mixed density + Mild enhancement	0.58	0.008
Orbital Tumors	Iso-dense + Moderate enhancement	0.72	0.002

Table 4.7: Further analysis at the subtype level revealed characteristic CT signatures for each tumor subtype, demonstrating strong to very strong correlations. Paraganglioma showed the highest correlation ($r=0.82$, $p<0.001$) with the combination of iso-density and calcification. Meningiomas also exhibited a very strong correlation ($r=0.81$, $p<0.001$) with hyperdensity and calcification. Metastatic breast tumors were strongly correlated with the presence of strong enhancement and necrosis ($r=0.72$, $p<0.001$). These findings underscore the diagnostic value of specific combinations of CT features in differentiating tumor subtypes, thereby further addressing the third research objective.

Table 4.8: CT Feature Co-occurrence Patterns

Feature Pair	Overall Co-occurrence	Most Common in	Statistical Significance (χ^2, p)
Strong Enhancement + Necrosis	18/52 (34.6%)	Metastatic tumors (66.7%)	$\chi^2 = 12.45$, p = 0.001
Hyperdensity + Calcification	6/52 (11.5%)	Meningiomas (75.0%)	$\chi^2 = 8.23$, p = 0.004
Hypodensity + Edema	14/52 (26.9%)	Primary gliomas (60.0%)	$\chi^2 = 7.89$, p = 0.007
Iso-density + Moderate Enhancement	8/52 (15.4%)	Orbital tumors (100%)	$\chi^2 = 10.12$, p = 0.002
Mixed Density + Mild Enhancement	4/52 (7.7%)	Metastatic skin (75.0%)	$\chi^2 = 6.45$, p = 0.012

Table 4.8: Significant co-occurrence patterns of CT features were identified, providing further diagnostic specificity. The combination of strong enhancement and necrosis was most frequently observed in metastatic tumors (66.7% of cases with this feature pair) and demonstrated strong statistical significance ($\chi^2 = 12.45$, p = 0.001). Hyperdensity combined with calcification was characteristic of meningiomas (75.0% of cases with this feature pair, $\chi^2 = 8.23$, p = 0.004). Similarly, hypodensity with edema was most prevalent in primary gliomas (60.0% of cases with this feature pair, $\chi^2 = 7.89$, p = 0.007). These co occurrence patterns significantly enhance the diagnostic utility of CT imaging and support the potential development of a robust diagnostic algorithm. enhance the diagnostic utility of CT imaging and support the potential development of a robust diagnostic algorithm.

4.7 Age and Gender Correlations with Tumor Types

This section explores the correlations between age, gender, and specific tumor types.

Table 4.9: Age and Gender Correlations with Tumor Types

Variable	Correlation with Age (r)	Correlation with Gender (r)	Most Associated Tumor Type
Primary CNS	-0.28	0.18	Pediatric/Young Adult
Metastatic	0.42*	0.25	Middle-aged/Older
Paraganglioma	-0.35	-0.45*	Young/Middle-aged Males
Hematologic	-0.18	0.23	Middle-aged Female
Orbital	-0.22	0.18	Variable Age, Slight Female

- $p < 0.05$

Table 4.9: Age demonstrated a significant positive correlation with metastatic tumors ($r=0.42$, $p<0.05$), confirming their higher prevalence in older patient populations. Conversely, a negative correlation was observed between age and paraganglioma ($r=-0.35$), although this did not reach statistical significance. Gender correlation (r) was statistically significant for paraganglioma ($r =-0.45$, $p<0.05$), which corroborates the male predominance observed for this tumor type. These correlations highlight the influence of demographic factors on the prevalence of specific tumor types.

4.2. Discussion

The present study provides a comprehensive analysis of the demographic characteristics and multi-parametric CT imaging features of brain and skull tumors in a Yemeni cohort from the National Oncology Center, Sana'a. The female predominance observed in our cohort (65.4%) aligns with several studies from the region and comparable settings. Bintang *et al*. (2024) reported a similar female predominance (64.4%) among 104 intracranial tumor patients in Indonesia. This finding may reflect the higher incidence of tumors with female predilection, such as meningiomas, which constituted 7.7% of our cases and are known to be influenced by hormonal factors (New *et al*., 1980). Additionally, breast cancer was identified as the most common primary source of metastases (17.3%), further contributing to the female predominance. Conversely, a recent neurosurgical study from Yemen by Al-Asadi *et al*. (2025) reported a male predominance (60.4%) among 96 primary brain tumor patients undergoing surgery. This discrepancy is likely explained by differences in study populations; their cohort focused exclusively on surgical primary brain tumor cases, whereas our study included both primary and metastatic tumors across all age groups at an oncology referral center. The inclusion of breast cancer metastases in our sample naturally elevates the female proportion.

The mean age of patients with metastatic tumors (50.8 ± 17.9 years) was significantly higher than those with primary CNS tumors (40.1 ± 20.3 years) ($p=0.001$). This finding is consistent with Sakdullah and Yueniwati (2025), who reported that brain metastases predominantly occur in patients aged 41-70 years, with a median age of 51 years. Fink and Fink (2013) similarly noted that metastatic tumors peak in the fifth and sixth decades, reflecting the age incidence of primary systemic cancers. The younger mean age for primary CNS tumors (40.1 years) in our study aligns with Al-Asadi *et al*. (2025), who reported a median age of 35 years (range 0.5-80) for primary brain tumor patients in Yemen. This younger demographic compared to Western populations may reflect the overall younger population structure in Yemen, where the median age is approximately 20 years, as well as potential differences in environmental exposures or genetic susceptibility.

Metastatic tumors constituted the largest category (46.2%) in our cohort, followed by primary CNS tumors (40.4%). This finding contrasts with Bintang *et al*. (2024), who reported that 88.5% of intracranial tumors in their Indonesian series were primary. This discrepancy may be attributed to the specialized nature of our study setting—the National Oncology Center, which serves as the primary referral center for cancer patients nationwide. Patients with known systemic malignancies are routinely referred for evaluation of suspected brain metastases, potentially enriching the sample with metastatic cases. Among metastatic tumors, breast cancer was the predominant primary source (17.3% of total cohort), followed by nasopharyngeal carcinoma (9.6%). This distribution differs from Sakdullah and Yueniwati (2025), who identified lung cancer as the most common source of brain metastases, followed by breast cancer. The high proportion of nasopharyngeal carcinoma in our series likely reflects regional variations in cancer epidemiology, as nasopharyngeal carcinoma has a relatively higher incidence in parts of the Middle East and North Africa. Within primary CNS tumors, gliomas/astrocytomas (9.6%) and meningiomas (7.7%) were most common, consistent with global literature (Ostrom *et al*., 2020). Al-Asadi *et al*. (2025) similarly found meningioma (19.8%) and glioblastoma (14.6%) as the predominant histologies among surgical primary brain tumor cases in Yemen.

The cerebral region was the most common location overall (48.1%), with metastatic tumors demonstrating higher skull involvement (41.7%) compared to non-metastatic tumors (28.6%). Supratentorial predominance (78%) was also reported by Al-Asadi *et al*. (2025) in the Yemeni surgical series and by Bintang *et al*. (2024) (74%). Multiple lesion involvement was significantly more frequent in metastatic tumors (54.2%) than in primary CNS tumors (28.6%) (p=0.002). This finding corroborates Sakdullah and Yueniwati (2025), who reported that most patients with brain metastases had multiple nodules. The multifocal nature of metastatic disease reflects hematogenous dissemination and serves as a valuable diagnostic clue, as noted by Fink and Fink (2013). The statistical significance of this association (χ^2 = 15.23, p = 0.002) underscores its utility in differentiating tumor types on CT imaging.

The analysis of CT imaging characteristics revealed distinct patterns across tumor types. Iso-dense lesions were characteristic of paraganglioma (100%), hematologic tumors (100%), and orbital tumors (100%). This finding aligns with Casselman *et al*. (2019), who

described paragangliomas as typically isodense on non-contrast CT. Hyperdensity was significantly correlated with primary CNS tumors ($r=0.42$, $p<0.05$), particularly meningiomas. New *et al*. (1980) similarly identified hyperdensity as a classic feature of meningiomas on non-contrast CT, attributable to their high cellularity and frequent calcification. Strong enhancement was observed in 100% of paraganglioma and hematologic tumors, and in 57.1% of primary CNS tumors. The correlation between strong enhancement and paraganglioma ($r=0.65$, $p<0.05$) is consistent with the known hypervascular nature of these tumors, which demonstrate intense enhancement on both CT and MRI (Rao *et al*., 1999; Rigby & Jackler, 1996).

Necrosis was most prevalent in metastatic tumors (70.8%), with a significant positive correlation ($r=0.45$, $p<0.05$). The co-occurrence of strong enhancement with necrosis was particularly characteristic of metastatic tumors (66.7% of cases with this feature pair, $p=0.001$). This finding aligns with Smirniotopoulos *et al*. (2007), who described ring enhancement with central necrosis as a common pattern in rapidly growing malignant lesions, including metastases and high-grade gliomas. Calcification was a hallmark feature of paraganglioma (100%) and was significantly correlated with this tumor type ($r=0.82$, $p<0.01$). While paraganglioma calcification is less frequently emphasized in the literature compared to other tumors, Casselman *et al*. (2019) noted that calcification can occur. Among primary CNS tumors, meningiomas demonstrated calcification in 42.9% of cases, consistent with Greenberg *et al*. (1999), who reported calcification in 20–30% of meningiomas. Perilesional edema and mass effect were common findings across most tumor categories (61.5% and 75.0%, respectively). Bintang *et al*. (2024) similarly reported perifocal edema as the most common radiological feature (66.3%) in their series. The absence of mass effect in orbital tumors reflects the unique anatomical constraints of the orbit, where tumors may cause proptosis before significant mass effect on intracranial structures.

The correlation analysis revealed several statistically significant associations that enhance the diagnostic utility of CT imaging. Paraganglioma demonstrated the strongest correlations, with iso-density ($r=0.68$, $p<0.05$), strong enhancement ($r=0.65$, $p<0.05$), and calcification ($r=0.82$, $p<0.01$). This distinctive CT signature may facilitate accurate pre-operative diagnosis, guiding appropriate surgical planning. Orbital tumors showed

significant correlation with iso-density ($r=0.72$, $p<0.05$) and moderate enhancement, providing a characteristic imaging profile. Metastatic tumors correlated significantly with necrosis ($r=0.45$, $p<0.05$), and the co-occurrence of strong enhancement with necrosis demonstrated strong statistical significance ($p=0.001$), serving as a valuable diagnostic marker. Meningiomas exhibited significant correlation with hyperdensity ($r=0.42$, $p<0.05$) and the co-occurrence of hyperdensity with calcification ($p=0.004$), confirming the findings of New *et al*. (1980). These findings support the hypothesis that specific CT imaging features are significantly associated with particular tumor types and that metastatic tumors demonstrate higher rates of multiplicity and necrosis compared to primary CNS tumors.

The diagnostic accuracy of CT in our study, inferred from significant correlations between imaging features and tumor types, supports the utility of CT as a primary diagnostic tool in resource-limited settings. This is particularly relevant in Yemen, where access to MRI is severely restricted due to economic and infrastructural constraints (Al-Asadi *et al*., 2025). Iqbalawati *et al*. (2025) recently demonstrated that CT findings of tumor density and wall characteristics show significant association with histopathological results ($p<0.05$), with 59% sensitivity and 75% specificity for determining malignancy. Their study concluded that CT provides valuable predictive information on intracranial tumor characteristics, showing significant concordance with histopathology. While MRI remains the gold standard for soft tissue characterization, Zhang (2025) found that MRI had superior diagnostic performance (sensitivity 96.83%, accuracy 96.05%) compared to CT (sensitivity 77.78%, accuracy 76.32%) for intracranial tumors. However, the same study acknowledged that CT remains valuable, particularly in specific clinical scenarios. Zhao *et al*. (2017) found no statistically significant difference in diagnostic accuracy between CT and MRI for skull base communicating tumors, though CT was superior for evaluating bone invasion. These findings underscore that while MRI offers advantages in tissue characterization, CT—when interpreted with attention to multi-parametric features—provides diagnostically useful information that can guide clinical management in settings where MRI is unavailable.

The severe healthcare challenges in Yemen, characterized by chronic power outages, critical supply shortages, and limited access to advanced imaging, have been well-documented (Al-Asadi *et al*., 2025). Despite these constraints, Al-Asadi *et al*. (2025)

demonstrated that strategic adaptive protocols enabled the achievement of neurosurgical outcomes comparable to other low-resource settings, with a six-month survival rate of 75%. Our study contributes to this effort by providing baseline radiological data that can inform diagnostic algorithms tailored to the Yemeni context. The characteristic CT signatures identified—such as the combination of iso-density, strong enhancement, and calcification for paraganglioma, or strong enhancement with necrosis for metastases—provide practical diagnostic clues that can be applied by radiologists and clinicians working with limited resources. The development of a preliminary CT-based diagnostic algorithm, as proposed in this study, aligns with the recommendation of Iqbalawati *et al*. (2025) that imaging protocols should be optimized for local contexts and resource availability.

Chapter five

Conclusions

5.1. Conclusions

- The study population demonstrated a significant female predominance (65.4%), with metastatic tumors occurring in older patients (mean age 50.8 years) compared to primary CNS tumors (mean age 40.1 years).
- Metastatic tumors were the most frequent category (46.2%), followed by primary CNS tumors (40.4%), with breast cancer identified as the most common primary source of metastases (17.3%).
- The cerebral region was the most common anatomical location overall (48.1%), while skull involvement was significantly higher in metastatic tumors (41.7%) compared to non-metastatic tumors (28.6%).
- Multiple lesion involvement was substantially more frequent in metastatic tumors (45.8%) than in non-metastatic tumors (25.0%), supporting the multifocal nature of metastatic disease.
- Specific CT imaging features showed characteristic patterns, such as iso-density in paraganglioma, hematologic, and orbital tumors, and strong enhancement in paraganglioma and hematologic tumors.
- Necrosis was most prevalent in metastatic tumors (70.8%), while calcification was a hallmark feature of paraganglioma (100%) and meningiomas.
- Statistically significant correlations were established between CT features and tumor types, notably paraganglioma with iso-density ($r=0.68$) and calcification ($r=0.82$), and orbital tumors with iso-density ($r=0.72$).
- Significant co-occurrence patterns, such as strong enhancement with necrosis in metastatic tumors ($p=0.001$) and hyperdensity with calcification in meningiomas ($p=0.004$), enhance the diagnostic specificity of CT imaging.

Chapter six

Recommendation

6.2. Recommendation

- The identified CT imaging signatures provide a robust empirical basis for developing a preliminary diagnostic algorithm suitable for resource-limited settings.
- Continuous professional development programs should be implemented for radiologists to enhance the recognition of these characteristic CT patterns and improve diagnostic accuracy.
- Localized, CT-based diagnostic protocols should be developed to guide clinical management in settings where histopathological confirmation is not immediately available.
- Clinicians should systematically incorporate patient demographic data, such as age and gender, into the differential diagnosis process for brain and skull tumors.
- Investment in accessible and well-maintained CT scanning infrastructure should be prioritized in underserved regions to facilitate early detection.
- Public health awareness campaigns should be launched to educate the population on early symptoms of brain tumors, targeting high-risk demographic groups.
- Future research should focus on prospective studies to quantitatively assess diagnostic performance metrics like sensitivity and specificity against histopathological standards.
- The integration of artificial intelligence and machine learning algorithms for automated CT interpretation should be explored to support radiologists in high-volume environments.
- Longitudinal studies are recommended to correlate initial CT findings with treatment responses and long-term patient outcomes.

References

References

1) Al-Asadi, M. Y. M., et al. (2025). Defying Deprivation: Neurosurgical Outcomes and 75% Six-Month Survival in 96 Primary Brain Tumor Cases Amid Yemen's Humanitarian Crisis. World Neurosurgery, 124526.
2) American Society of Clinical Oncology. (2022). Computed tomography (CT) scan. Cancer.Net. Retrieved [access date if known, otherwise use "n.d."], from https://www.cancer.net/navigating-cancer-care/diagnosing-cancer/tests-and-procedures/computed-tomography-ct-scan
3) Arora, A., *et al*. (2022). Imaging of Skull Base Tumors: A Comprehensive Review. Neuroimaging Clinics of North America, 32(2), 351-370.
4) Atlas, S. W. (1990). Magnetic Resonance Imaging of the Brain and Spine. Raven Press.
5) Bae, K. T. (2010). Intravenous Contrast Medium Administration and Scan Timing at CT: Considerations and Approaches. Radiology, 256(1), 32–61.
6) Bae, K. T. (2010). Intravenous Contrast Medium Administration and Scan Timing at CT: Considerations and Approaches. Radiology, 256(1), 32–61.
7) Bintang, K. S., Novirianthy, R., & Hidayaturrahmi, H. (2024). Imaging Profile of Intracranial Tumors at Dr. Zainoel Abidin Regional General Hospital Banda Aceh. Indonesian Journal of Cancer, 18(2).
8) Bondy, M. L., Scheurer, M. E., Malmer, B., Barnholtz-Sloan, J. S., Davis, F. G., Il'yasova, D., ... & Brain Tumor Epidemiology Consortium. (2008). Brain tumor epidemiology: Consensus from the Brain Tumor Epidemiology Consortium. Cancer, 113(7 Suppl), 1953-1968.
9) Brant-Zawadzki, M., Norman, D., Newton, T. H., Kelly, W. M., Kjos, B., Mills, C. M., Dillon, W. P., Sobel, D., & Crooks, L. E. (1984). Magnetic Resonance Imaging of the Brain: The Optimal Screening Technique. Radiology, 152(1), 71–77.
10) Buhl, R., Barth, H., Hugo, H. H., Mautner, V. F., & Mehdorn, H. M. (2004). Intracranial and spinal melanotic schwannoma in the same patient. Journal of Neuro-Oncology, 68(3), 249–254. https://doi.org/10.1023/B:NEON.0000033491.23654.6c

11) Casselman, J. W., De Jonge, I., Neyt, L., De Clercq, C., & D'Hont, G. (1993). MRI in craniofacial fibrous dysplasia. Neuroradiology, 35(3), 234–237. https://doi.org/10.1007/BF00588505
12) Casselman, J. W., Vanden Bossche, S., Pretorius, E., & De Foer, B. (2019). Skull-base tumors and related disorders. In F. Barkhof, R. Jager, M. Thurnher, & A. Rovira Cañellas (Eds.), Clinical neuroradiology. Springer. [DOI]
13) Casselman, J., et al. (2019). Imaging of the Skull Base. In Skull Base Imaging. Elsevier.
14) Chang, J. E., Khuntia, D., Robins, H. I., & Mehta, M. P. (2007). Radiotherapy and radiosensitizers in the treatment of glioblastoma multiforme. Clinical Advances in Hematology & Oncology, 5(11), 894-902.
15) Chowdhury, F. H., Haque, M. R., Kawsar, K. A., Sarker, M. H., Hasan, M., & Goel, A. H. (2014). Intracranial nonvestibular neurinomas: Young neurosurgeons' experience. Journal of Neurosciences in Rural Practice, 5(3), 231–243. https://doi.org/10.4103/0976-3147.133566
16) Clark, W. C., *et al*. (1985). Brain tumors in children. Neurologic Clinics, 3(4), 787-802.
17) Clarke, C. R. A. (2005). Neurological diseases. In P. Kumar & M. Clark (Eds.), Kumar & Clark clinical medicine (6th ed., pp. 1244-1245). Elsevier Saunders.
18) Dahlen, R. T., Johnson, C. E., Harnsberger, H. R., Biediger, C. P., Syms, C. A., Fischbein, N. J., & Schwartz, J. M. (2002). CT and MR imaging characteristics of intravestibular lipoma. American Journal of Neuroradiology, 23(8), 1413–1417.
19) Dandy, W. E. (1918). Ventriculography following the injection of air into the cerebral ventricles. Annals of Surgery, 68(1), 5-11.
20) Dolecek, T. A., Propp, J. M., Stroup, N. E., & Kruchko, C. (2012). CBTRUS statistical report: Primary brain and central nervous system tumors diagnosed in the United States in 2005-2009. Neuro-Oncology, 14(Suppl 5), v1-v49.
21) Ellika, S. K., Jain, R., Patel, S. C., Scarpace, L., Schultz, L. R., Rock, J. P., & Mikkelsen, T. (2007). Role of Perfusion CT in Glioma Grading and Comparison with Conventional MR Imaging Features. American Journal of Neuroradiology, 28(10), 1981–1987.

22) Farid, N. (2014). Imaging of vestibular schwannoma and other cerebellopontine angle tumors. Operative Techniques in Otolaryngology-Head and Neck Surgery, 25(1), 87–95. https://doi.org/10.1016/j.otot.2013.11.011
23) Fink, K. R., & Fink, J. R. (2013). Imaging of brain metastases. Surgical Neurology International, 4(Suppl 4), S209-S219.
24) Fink, K. R., & Fink, J. R. (2013). Imaging of brain metastases. Surgical Neurology International, 4(Suppl 4), S209-S219.
25) Fujimoto, K., Ohnishi, H., Tsujimoto, M., Hashida, T., & Nakazato, Y. (2000). Dysembryoplastic neuroepithelial tumors of the cerebellum and brainstem. Journal of Neurosurgery, 93(3), 487-489.
26) Furie, D. M., & Provenzale, J. M. (1995). Supratentorial ependymomas and subependymomas: CT and MR appearance. Journal of Computer Assisted Tomography, 19(4), 518-526.
27) Gillies, R. J., Kinahan, P. E., & Hricak, H. (2016). Radiomics: Images Are More than Pictures, They Are Data. Radiology, 278(2), 563–577.
28) Gomez, C. K., *et al*. (2018). Calcified brain tumors: A practical imaging review. Radiographics, 38(3), 894-910.
29) Greenberg, H. S., *et al*. (1999). Handbook of Neurosurgery. Thieme.
30) Greenberg, H. S., et al. (1999). Handbook of Neurosurgery. Thieme.
31) Hoang-Xuan, K., Bessell, E., Bromberg, J., Hottinger, A. F., Preusser, M., Rudà, R., ... & European Association for Neuro-Oncology Task Force on Primary CNS Lymphoma. (2015). Diagnosis and treatment of primary CNS lymphoma in immunocompetent patients: Guidelines from the European Association for Neuro-Oncology. The Lancet Oncology, 16(7), e322-e332.
32) Houillier, C., Choquet, S., Touitou, V., Martin-Duverneuil, N., Navarro, S., Mokhtari, K., ... & Hoang-Xuan, K. (2015). Lenalidomide monotherapy as salvage treatment for recurrent primary CNS lymphoma. Neurology, 84(3), 325-326.
33) Iida, E., & Anzai, Y. (2017). Imaging of paranasal sinuses and anterior skull base and relevant anatomic variations. Radiologic Clinics of North America, 55(1), 31–52. https://doi.org/10.1016/j.rcl.2016.08.009

34) Iqbalawati, I., et al. (2025). Intracranial tumors on CT and MRI: The association of imaging characteristics with histopathological findings. Bali Medical Journal, 14(3).
35) Korfel, A., Thiel, E., Martus, P., Möhle, R., Griesinger, F., Rauch, M., ... & Fischer, L. (2015). Randomized phase III study of whole-brain radiotherapy for primary CNS lymphoma. Neurology, 84(12), 1242-1248.
36) Kurokawa, R., *et al*. (2022). Imaging of Oligodendroglioma: A Review of the 2021 WHO Classification. Japanese Journal of Radiology, 40(7), 661-673.
37) Kushchayeva, Y. S., Kushchayev, S. V., Glushko, T. Y., Tella, S. H., Teytelboym, O. M., Collins, M. T., & Boyce, A. M. (2018). Fibrous dysplasia for radiologists: Beyond ground glass bone matrix. Insights into Imaging, 9(6), 1035–1056. https://doi.org/10.1007/s13244-018-0666-6
38) Laigle-Donadey, F., Taillibert, S., Martin-Duverneuil, N., Hildebrand, J., & Delattre, J.-Y. (2005). Skull-base metastases. Journal of Neuro-Oncology, 75(1), 63–69. https://doi.org/10.1007/s11060-004-8099-0
39) Liu, X.-D., Xu, Q.-W., Che, X.-M., & Yang, D.-L. (2009). Trigeminal neurinomas: Clinical features and surgical experience in 84 patients. Neurosurgical Review, 32(4), 435–444. https://doi.org/10.1007/s10143-009-0210-8
40) MacNally, S. P., Rutherford, S. A., Ramsden, R. T., Evans, D. G., & King, A. T. (2008). Trigeminal schwannomas. British Journal of Neurosurgery, 22(6), 729–738. https://doi.org/10.1080/02688690802272172
41) Matias, T. B., Cordeiro, R. A., Duarte, J. A., de Jarry, V. M., Appenzeller, S., Villarinho, L., & Reis, F. (2023). Immune-mediated hypertrophic pachymeningitis and its mimickers: Magnetic resonance imaging findings. Academic Radiology, 30(8), 1675-1686. Advance online publication. https://doi.org/10.1016/j.acra.2023.01.017
42) McNamara, C., *et al*. (2022). An overview of the cIMPACT-NOW updates and the 2021 WHO Classification of CNS Tumors for practicing radiologists. Neuroradiology, 64(8), 1471-1487.
43) Moffat, D. A., & Ballagh, R. H. (1995). Rare tumours of the cerebellopontine angle. Clinical Oncology, 7(1), 28–41. https://doi.org/10.1016/S0936-6555(05)80632-6

44) Nelson, M., Diebler, C., & Forbes, W. S. (1991). Paediatric medulloblastoma: Atypical CT features at presentation in the SIOP II Trial. Neuroradiology, 33(2), 140-142.

45) New, P. F., *et al*. (1980). Computed tomography of meningiomas. Journal of Computer Assisted Tomography, 4(4), 424-435.

46) New, P. F., et al. (1980). Computed tomography of meningiomas. Journal of Computer Assisted Tomography, 4(4), 424-435.

47) Nikolopoulos, T. P., Fortnum, H., O'Donoghue, G., & Baguley, D. (2010). Acoustic neuroma growth: A systematic review of the evidence. Otology & Neurotology, 31(3), 478–485. https://doi.org/10.1097/MAO.0b013e3181d279a3

48) Ohgaki, H., & Wiestler, O. D. (2007). The 2007 WHO classification of tumors of the central nervous system. Acta Neuropathologica, 114(2), 97-109.

49) Ostrom, Q. T., Patil, N., Cioffi, G., Waite, K., Kruchko, C., & Barnholtz-Sloan, J. S. (2020). CBTRUS Statistical Report: Primary Brain and Other Central Nervous System Tumors Diagnosed in the United States in 2013–2017. Neuro-Oncology, 22(Supplement_1), iv1–iv96.

50) Ostrom, Q. T., Patil, N., Cioffi, G., Waite, K., Kruchko, C., & Barnholtz-Sloan, J. S. (2020). CBTRUS Statistical Report: Primary Brain and Other Central Nervous System Tumors Diagnosed in the United States in 2013–2017. Neuro-Oncology, 22(Supplement_1), iv1–iv96.

51) Paldino, M. J., Faerber, E. N., & Poussaint, T. Y. (2011). Imaging tumors of the pediatric central nervous system. Radiologic Clinics of North America, 49(4), 589-616.

52) Rao, A. B., et al. (1999). Imaging of paragangliomas of the head and neck. Neuroimaging Clinics of North America, 9(3), 525-543.

53) Rao, A. B., Koeller, K. K., & Adair, C. F. (1999). From the archives of the AFIP: Paragangliomas of the head and neck—Radiologic-pathologic correlation. RadioGraphics19(6),1605–1632. https://doi.org/10.1148/radiographics.19.6.g99no251605

54) Rigby, P. L., & Jackler, R. K. (1996). Clinicopathologic presentation and diagnostic imaging of jugular foramen tumors. Operative Techniques in Otolaryngology–Head and Neck Surgery, 7(2), 99–105. https://doi.org/10.1016/S1043-1810(96)80021-2

55) Rigby, P. L., & Jackler, R. K. (1996). Imaging of glomus jugulare tumors. Otolaryngologic Clinics of North America, 29(3), 439-456.

56) Sakdullah, I., & Yueniwati, Y. (2025). Demographic Profile and CT-MRI Characteristics of Brain Metastasis Patients at Dr Saiful Anwar Hospital: A Retrospective Study. International Journal of Radiology and Imaging, 4(01), 7–17.

57) Silver, A. J., Ganti, S. R., & Hilal, S. K. (1982). Computed tomography of tumors involving the atria of the lateral ventricles. Radiology, 145(1), 71-78.

58) Skolnik, A. D., Loevner, L. A., Sampathu, D. M., Newman, J. G., Lee, J. Y., Bagley, L. J., & Learned, K. O. (2016). Cranial nerve schwannomas: Diagnostic imaging approach. RadioGraphics, 36(5), 1463–1477. https://doi.org/10.1148/rg.2016150199

59) Smirniotopoulos, J. G., Murphy, F. M., Rushing, E. J., Rees, J. H., & Schroeder, J. W. (2007). Patterns of Contrast Enhancement in the Brain and Meninges. RadioGraphics, 27(2), 525–551.

60) Smirniotopoulos, J. G., Murphy, F. M., Rushing, E. J., Rees, J. H., & Schroeder, J. W. (2007). Patterns of Contrast Enhancement in the Brain and Meninges. RadioGraphics, 27(2), 525–551.

61) Touitou, V., LeHoang, P., & Bodaghi, B. (2015). Primary CNS lymphoma. Current Opinion in Ophthalmology, 26(6), 526-533.

62) Tuan, A. S., Chen, J. Y., & Mafee, M. F. (2014). Glomus tympanicum and other intratympanic masses: Role of imaging. Operative Techniques in Otolaryngology–Head and Neck Surgery, 25(1), 49–57. https://doi.org/10.1016/j.otot.2013.11.007

63) Van Den Berg, R. (2005). Imaging and management of head and neck paragangliomas. European Radiology, 15(7), 1310-1318.

64) Vogl, T., & Bisdas, S. (2009). Differential diagnosis of jugular foramen lesions. Skull Base, 19(1), 3–16. https://doi.org/10.1055/s-0028-1103121

65) Wallace, E. W. (2004). The dural tail sign. Radiology, 233(1), 56–57. https://doi.org/10.1148/radiol.2331021332

66) WHO Classification of Tumours Editorial Board. (2020). Soft tissue and bone tumours (5th ed., Vol. 3). International Agency for Research on Cancer.

67) Zamora, C., & Castillo, M. (2017). Sellar and parasellar imaging. Neurosurgery, 80(1), 17–38. https://doi.org/10.1093/neuros/nyw013

68) Zhang, L., Yang, Y., Xu, S., Wang, J., Liu, Y., & Zhu, S. (2009). Trigeminal schwannomas: A report of 42 cases and review of the relevant surgical approaches. Clinical Neurology and Neurosurgery, 111(3), 261–269. https://doi.org/10.1016/j.clineuro.2008.10.014

69) Zhang, Y. (2025). CT [Application effect of CT and multi-modal MRI in the diagnosis of intracranial tumors]. Journal of Imaging Research and Medical Applications, 9(09), 135-137.

70) Zhao, et al. (2017). [Comparison of clinical features and diagnostic value of CT and MRI in patients with skull base communicating tumor]. Chinese Journal of Integrative Medicine and Imaging, (1).

Appendixes

Appendix I

(Data Collection Sheet)

Case	Age	Gender	Tumor Category	Primary Origin	Location	Multiplicity	CT Density	Enhancement	Necrosis	Calcification	Edema	Mass Effect
1												
2												
3												
4												
5												
6												
7												
8												
9												
10												
11												
12												
13												
14												
15												
16												
17												
18												
19												
20												
21												
22												
23												
24												
25												

26												
27												
28												
29												
30												
31												
32												
33												
34												
35												
36												
37												
38												
39												
40												
41												
42												
43												
44												
45												
46												
47												
48												
49												
50												
51												
52												

Arabic Summary

الملخص

الخلفية: تمثل أورام الدماغ والجمجمة أسبابًا رئيسية للمراضة العصبية. في البيئات محدودة الموارد مثل اليمن، حيث غالبًا ما يكون التصوير بالرنين المغناطيسي غير متوفر، يبقى التصوير المقطعي المحوسب الأداة التشخيصية الأساسية. ومع ذلك، تفتقر البيانات المنهجية حول خصائص هذه الأورام بالتصوير المقطعي لدى السكان اليمنيين. تهدف هذه الدراسة إلى تقييم الخصائص الديموغرافية وسمات التصوير المقطعي المحوسب متعددة المعايير لأورام الدماغ والجمجمة في المركز الوطني للأورام بصنعاء، اليمن.

المنهجية : أجريت دراسة وصفية مقطعية من أكتوبر 2025 إلى فبراير 2026، شملت 52 مريضًا متتاليًا (تتراوح أعمارهم بين 2 و 75 عامًا) تم تشخيص إصابتهم بأورام الدماغ أو الجمجمة وخضعوا للتصوير المقطعي المحوسب المعزز بالتباين. تم تحليل البيانات الديموغرافية وخصائص الورم وسمات التصوير المقطعي (الكثافة، التعزيز، النخر، التكلس، الوذمة، تأثير الكتلة) باستخدام برنامج SPSS الإصدار 23.0، مع تحديد مستوى الدلالة الإحصائية عند $p < 0.05$.

النتائج: غلبت الإناث على العينة (65.4٪). كانت الأورام النقيلية الأكثر شيوعًا (46.2٪)، تليها أورام الجهاز العصبي المركزي الأولية (40.4٪)؛ وكان سرطان الثدي المصدر الأساسي الأبرز (17.3٪). كانت المنطقة المخية الموقع التشريحي الأكثر شيوعًا (48.1٪). كانت الآفات المتعددة أكثر تكرارًا بشكل ملحوظ في النقائل (54.2٪) مقارنة بالأورام الأولية (28.6٪) ($p=0.002$) شملت الارتباطات الهامة: ورم المستقتمات مع تساوي الكثافة ($r=0.68$) والتكلس ($r=0.82$) الأورام المحجرية مع تساوي الكثافة ($r=0.72$) والنقائل مع النخر ($r=0.45$) كانت أنماط الترافق الرئيسية هي التعزيز القوي مع النخر في النقائل ($p=0.001$) وفرط الكثافة مع التكلس في الأورام السحائية .($p=0.004$)

الاستنتاج :يُظهر التصوير المقطعي المحوسب فعالية في توصيف أورام الدماغ والجمجمة في البيئات محدودة الموارد. توفر أنماط سمات التصوير المقطعي المميزة وارتباطاتها الإحصائية أساسًا لخوارزمية تشخيص أولية، مما يعزز التشخيص المبكر واتخاذ القرارات السريرية حيث يكون التصوير المتقدم أو الفحص النسيجي المرضي غير متوفرين.

الكلمات المفتاحية: أورام الدماغ، أورام الجمجمة، التصوير المقطعي المحوسب، اليمن، البيئات محدودة الموارد، علم أورام الأعصاب، الأورام النقيلية، الورم السحائي، ورم المستقتمات.

21 SEPTEMBER UNIVERSITY
OF MEDICAL & APPLIED SCIENCES
Deanship of Environment
and Community Service
Medical Center for Training
and Rehabilitation

جامعة ٢١ سبتمبر للعلوم الطبية والتطبيقية
عمادة البيئة وخدمة المجتمع
المركز الطبي للتدريب والتأهيل

التقييم الشعاعي لأورام الدماغ والجمجمة باستخدام التصوير المقطعي المحوسب

بحث مقدم لاستيفاء جزء من متطلبات الحصول على درجة الدبلوم في الأشعة التشخيصية

اعداد الباحثين

نجلاء نجيب احمد الحزمي — **صماط صالح محمد احمد الضبري**

ابرار عادل محمد احمد الشرجي — **ولاء احمد محمد صالح الغزالي**

دعاء حسين احمد العكاد — **يونس عبدالله محمد احمد القادري**

سعاد محمد قاسم الحاج القاسمي — **رديه عبدالواحد احمد الشيخ**

تحت اشراف

د/ ابراهيم الحمدي

د/ نور الدين الفقيه

2025-2026م